Hemodynamic Optimization of a Passive Assist Total Cavopulmonary Connector for ages 1-20

Elizabeth Mack

Thesis submitted to the Faculty of the
Virginia Polytechnic Institute and State University
in partial fulfillment of the requirements for the degree of

Master of Science
in

Engineering Mechanics

Alexandrina Untaroiu, Chair
Walter O'Brien
Anne Staples

June 25, 2018
Blacksburg, Virginia

Keywords: Cavopulmonary Assist Device, Computational Fluid Dynamics, Hemodynamics, Blood Damage

Hemodynamic Optimization of a Passive Assist Total Cavopulmonary Connector for ages 1-20

Elizabeth Kathleen Mack

Abstract

Currently, the surgical procedure followed by the majority of cardiac surgeons to address right ventricular dysfunction is the Fontan procedure, which connects the superior and inferior vena cava directly to the left and right pulmonary arteries bypassing the right atrium. However, this is not the most efficient configuration from a hemodynamics perspective. The goal of this study is to develop a patient-specific 4-way connector to bypass the dysfunctional right ventricle and augment the pulmonary circulation. The 4-way connector was intended to channel the blood flow from the inferior and superior vena cava directly to the right and left pulmonary arteries. By creating a connector with proper hemodynamic characteristics, one can control the jet flow interactions between the inferior and superior vena cava and streamline the flow towards the right and left pulmonary arteries. In this study, the focus was on creating a system that could identify the optimal configuration for the 4-way connector for patients from 1-20 years of age.

A platform was created in ANSYS that utilized the design of experiments (DOE) function to minimize power-loss and blood damage propensity in the connector based on junction geometries. A CFD model was created to simulate the blood flow through the connector. Then the geometry of the bypass connector was parameterized for the DOE process. The selected design parameters included inlet and outlet diameters, radius at the intersection, and length of the connector pathways. The chosen range for each geometric parameter was based on the relative size of the patient's arteries found in the literature. It was confirmed that as the patient's age and artery size change, the optimal size and shape of the connector also changes. However, the corner radius did not decrease at the same rate as the opening diameters. This means that creating different sized connectors is not just a matter of scaling the original connector to match the desired opening diameter. However, it was found that power losses within the connector decrease and average and maximum blood traversal time through the connector increased for increasing opening radius.

A follow up study was conducted to try to reduce or negate a consistent recirculation area found at the center of the connectors. To accomplish this a flow diverter was added to the center of the connector and optimized for each of the connectors found for the age groups used. From this study, it was found that the diverter did negate the recirculation area form the centers of the connectors. A separate Blood Damage Index (BDI) study was also run on this optimized connector with a diverter, the optimized connectors from the first study and a baseline connector. This showed a decrease in IVC sourced BDI for the optimized versions of the connector compared to the baseline geometries. This information could be used to create a more specific relationship between the opening radius and the flow characteristics. So in order to create patient specific connectors, either a new more complicated trend needs to be found or an optimization program would need to be run on each patient's specific geometry when they need a new connector.

Hemodynamic Optimization of a Passive Assist Total Cavopulmonary Connector for ages 1-20

Elizabeth Kathleen Mack

General Audience Abstract

Currently, the surgical procedure followed by the majority of cardiac surgeons to address a nonfunctioning right portion of the heart is the Fontan procedure, which connects the two major inflow venous structures from the right side of the heart directly to the two major outflow venous structures, bypassing the right nonfunctioning right portion of the heart. However, this is not the most efficient configuration from a fluid flow perspective. The goal of this study is to develop a patient-specific 4-way connector to bypass the nonfunctioning right side of the heart and aid in overall circulation. Just like the Fontan procdure, the 4-way connector was intended to channel the blood flow from the two main inflow venous structures directly to the two major outflow venous structures. By creating a connector with proper fluid flow characteristics, one can control the flow interactions between the two inflows and streamline the flow towards the two outflow venous structures. In this study, the focus was on creating a system that could identify the optimal configuration for the 4-way connector for patients from 1-20 years of age.

A platform was created in a modeling and simulation program, called ANSYS, that utilized the design of experiments (DOE) function to minimize power-loss and the likelihood of blood damage in the connector based on connector geometries. A CFD model was created to simulate the blood flow through the connector. Then the geometry of the bypass connector was parameterized for the DOE process. The selected design parameters included inlet and outlet diameters, radius at the intersection, and length of the connector pathways. The chosen range for each geometric parameter was based on the relative size of the patient's arteries found in the literature. It was confirmed that as the patient's age and artery size change, the optimal size and shape of the connector also changes. From the results of the first study showed a very decreasing relationship between the opening radius and the corner radius as the opening radius increased in size. It was also found that power losses within the connector decrease and average and maximum blood traversal time through the connector increased for increasing opening radius.

A follow up study was conducted to try to reduce or negate a consistent recirculation area found at the center of the connectors. To accomplish this a flow diverter was added to the center of the connector and optimized for each of the connectors found for the age groups used. From this study, it was found that the diverter did negate the recirculation area form the centers of the connectors. A separate Blood Damage Index (BDI) study was also run on this optimized connector with a diverter, the optimized connectors from the first study and a baseline connector. This showed a decrease in BDI from the venous structure with the larger inlet flow for the optimized versions of the connector compared to the baseline geometries. This information could be used to create a more specific relationship between the opening radius and the flow characteristics. So in order to create patient specific connectors, either a new more complicated trend needs to be found or an optimization program would need to be run on each patient's specific geometry when they need a new connector.

Acknowledgements

I would like to take this time to thank some very important people, without whom this thesis would not have been completed. First, I would like to thank my committee members, Dr. Alexandrina Untaroiu, Dr. Anne Staples, and Dr. Walter O'Brien. Thank you for being patient with me and being willing to support me in this, even though the actually creation of the thesis was so short notice. A special thanks to Dr. Untaroiu, my committee chair, for all of the helpful suggestions and edits. I may not always be the easiest person to work with, but thank you for sticking it out with me.

I would also like to thank my wonderful parents, Stephenie and Robin Mack, and my little sister, Marie, for all of their support though this part of my journey. Sometimes just knowing there are people there who love and support you makes all the difference, and the added help of extra food and listening ears is icing on the cake. Thank you for being there for me.

I would also like to thank all of the people in the VT ESM department for helping an encouraging me along the way. I have truly been blessed to have had the opportunity to work along side you for these past 7 years, in my time as an undergraduate or after I became a graduate student. The ESM Department has felt like a family, so thank you all from the bottom of my heart.

Last but not least, I want to thank the love of my life, Josh Vaught. I don't know what I would have done without you.

Table of Contents

Chapter 1

1 Introduction

1.1 Motivation

Congenital heart defects affect more than 1.3 million living Americans today. Additionally, each year about 40,000 children are born with a heart defect. Congenital heart defects are the most common type of birth defect and are characterized by an underdeveloped or malformed heart muscle, valve, or chamber [1]. Unfortunately, about 30 -50% of all deaths associated with congenital heart defects are in infants [2]. Single ventricle heart defects are one of the most complicated heart defects. A single ventricle heart defect is one where either of the ventricles are underdeveloped, weak, or non-functions. This affects blood circulation and re-oxygenation in the body. Though this kind of defect is rare, corrective action usually requires at least one surgery [3]. This study will be focusing on creating a connector geometry for patients suffering from right ventricular dysfunction. Currently, the surgical procedure followed by the majority of cardiac surgeons for this kind of failure is the Fontan procedure, which connects the superior vena cava (SVC) and the inferior vena cava (IVC) directly to the left and right pulmonary arteries (LPA and RPA respectively) bypassing the right atrium. Though this procedure has been found to have an 85% survival rate at 20 years [4], because of the way the vessels are sutured together this type of connection is not the most efficient [5]. Any irregular or uneven surface within the sutured joint would contribute to the creation of recirculation and stagnation points as well as energy loss as the blood flows through the connection. Thus increasing the likelihood of thrombosis as well as the strain placed on the working left ventricle.

1.1.1 Normal vs. irregular

In order to understand and appreciate the difficulty of living with a heart defect, it is important to have a working idea of how a normal heart functions (see Figure 1). The heart is a muscle about the size of a fist that is split into the left and right sides. The right side of the heart deals with pumping the deoxygenated

blood to the lungs for re-oxygenation. The left side of the heart deals with pumping the oxygenated blood from the lungs to the rest of the body. Each side has two chambers and two one way valves. When the blood flows into the heart, it is first gathered in the first chamber (the atrium), then flows through one of the four valves into the second chamber (the ventricle). Then from the ventricle to either the lungs (as with the right side of the heart) or the rest of the body (as with the left side). In the case of single ventricle dysfunction, which is the heart defect looked at in this study, one of the ventricles is ether malformed or underdeveloped which decreases or disables the heart's ability to pump blood to or from the lungs. This not only decreases the efficiency of the dysfunctional ventricle, but also put more strain on the single functional side of the heart and lead to the inability to engage in higher level physical activity and other medical issues.

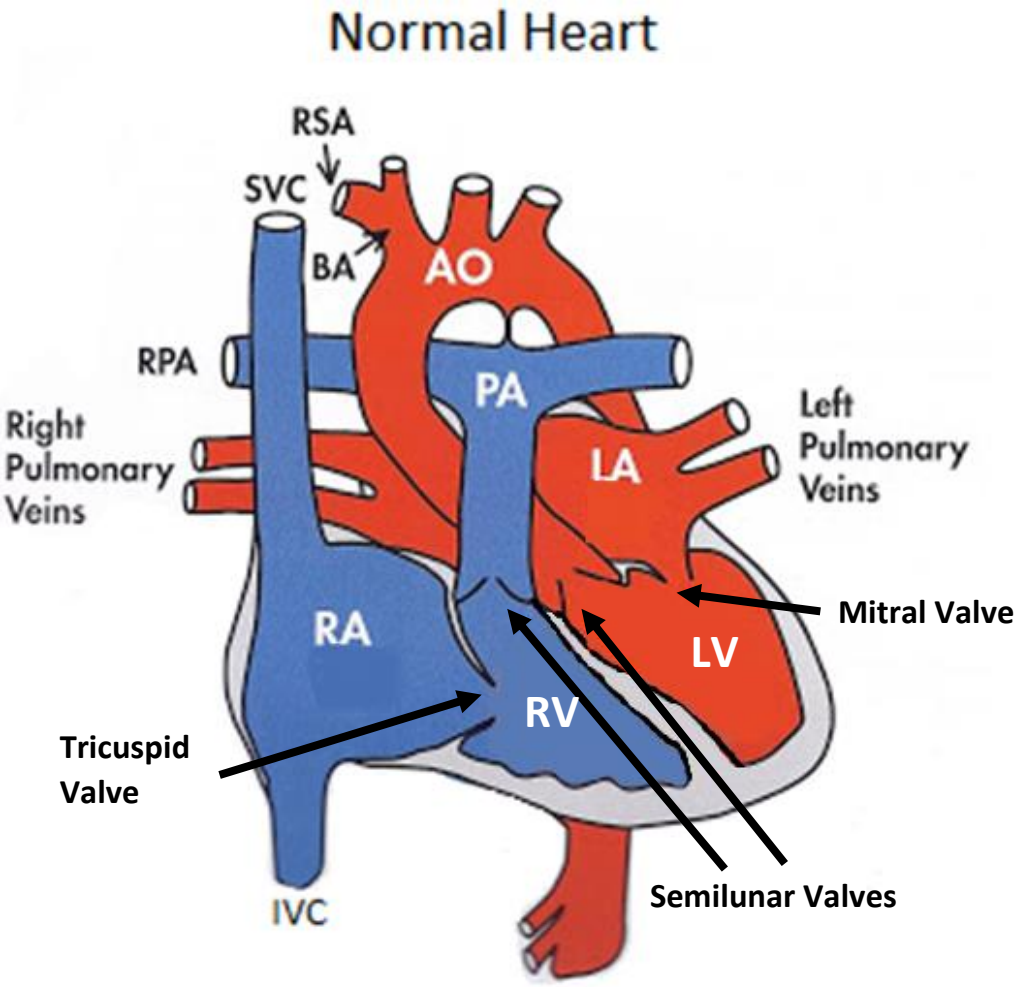

Figure 1: Normal heart where RA = Right Atrium, LA = Left Atrium, RV = Right Ventricle, LV = Left Ventricle.

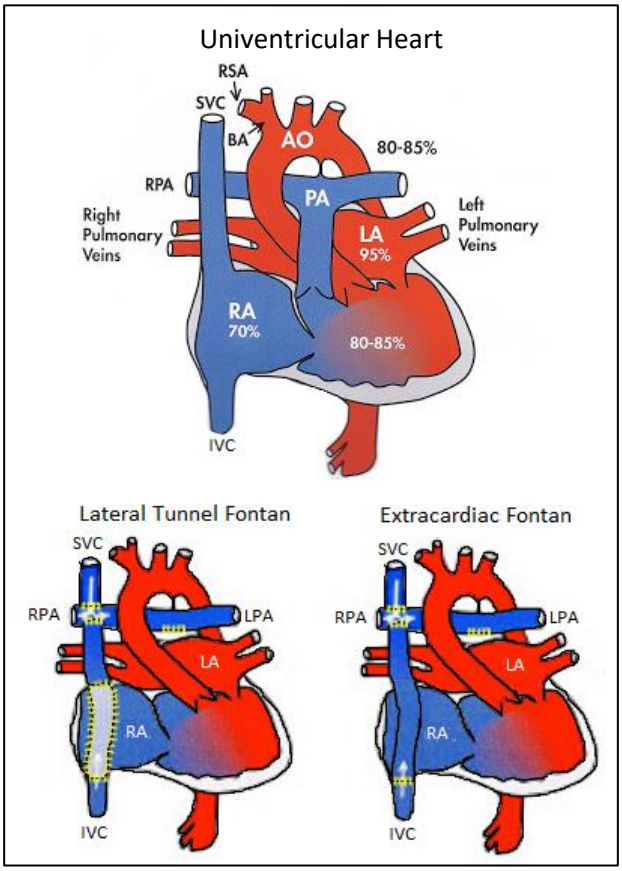

Figure 2. Univentricular heart geometry compared to Lateral Tunnel and Extracardiac Fontan configurations for univentricular heart

1.1.2 Current research

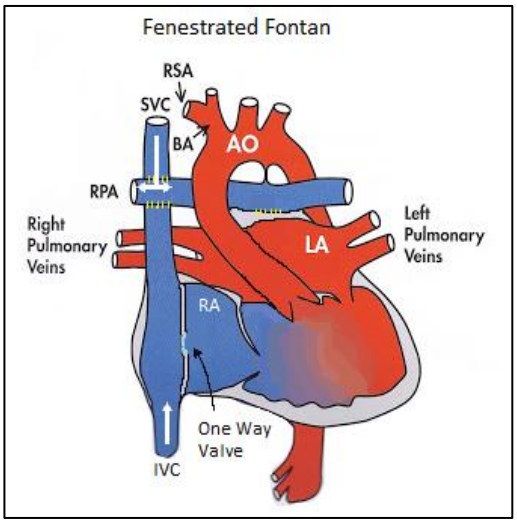

Figure 3. Fenestrated Fontan configuration for univentricular heart

The Fontan procedure was published in 1971 by F. Fontan and E. Baudet [6] as a correction surgery for tricuspid atresia, a case where the right side of the heart is underdeveloped or malformed. Now, the Fontan procedure is the most used procedure for right ventricular dysfunction corrective surgeries. Since its development, studies have been conducted to improve its design and long-term effects. [4, 7]. However, the vast majority of these alternative procedures deal with alternate ways of connecting the IVC to the RPA. These procedures include the Lateral Tunnel and Extra-cardiac Conduit configurations [4] as seen in Figure 2.

The most notable improvement is the Fenestrated Fontan procedure, which creates a small opening from the IVC to the right atrium to prevent overloading the connection [7]. This configuration is illustrated in Figure 3. The Fenestrated Fontan procedure can only be used in certain circumstances and is not always an option. Studies have also been done to determine the best alignment for the sutured vessels. Jagani and Untaroiu [8] investigated the effects of four different Fontan orientations on the hemodynamic

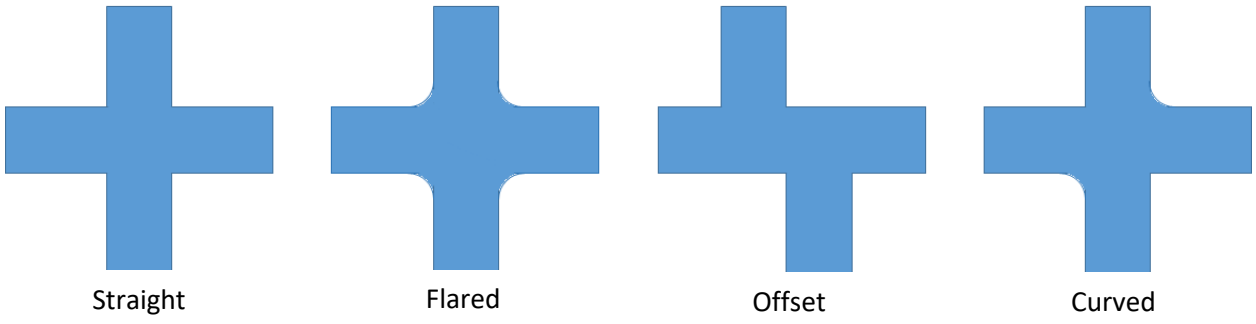

Figure 4. Cross sections of four different configurations for the four-way connection

characteristics and flow. The four configurations can be seen in Figure 4. The results from this study indicated that superior hemodynamics was exhibited by the flared configuration. However, it is very difficult to control the shape of and flow patterns through the connection when the blood vessels are sutured together. Variations in the patient's activity, internal anatomy, or the surgical methodology could affect the geometry of the connection in unpredictable and sometimes adverse ways. For example, the orientation of the sutured vessels for each Fontan procedure has been inconsistent, with some procedures suturing the vessels directly opposite each other and others suturing the vessels slightly offset from each other. This could lead to recirculation and stagnation areas within the connection, which could contribute to increased power losses and blood damage as well as the formation of clots that could cause stroke. Some studies have been conducted to find alternative ways of connecting the vessels to improve hemodynamics and decrease losses and damage. For example, Soerensen et al [9] tested a Total Cavopulmonary Connector (TCPC) designed to avoid the effects of dissipative inflow collision by branching the IVC and SVC into the LPA and RPA. This allowed for the smooth and even distribution of blood from the ICV and SVC into the LPA and RPA, leading to a decrease in power loss compared to the one diameter offset Fontan formation. Additionally, Marsden et al [10] evaluated a "y-shaped" connector in which the SVC ends in a T connection and the IVC ends in a "y-shaped" connection. The two branches of each were then routed to the LPA and RPA creating a triangle shaped branch connection. This formation with the wider "y" branches was shown to perform better than the one diameter offset in efficiency, IVC pressure, SVC pressure and flow distribution. However, these examples require making these complicated connections out of the available vasculature, which means longer surgeries and more suturing. The goal of this study is to optimize the flared configuration found by Jagani and Untaroiu to minimize power loss and recirculation and create a guide for printable passive flow assist devices based on this optimization. The final design would also be able to accommodate active flow assist elements to help enable a more normal level of physical activity for the patients.

A micro-pump that could work in conjunction with the connector has been investigated to address right ventricular dysfunction in the pediatric population [11, 12]. This initial work for device development was focused on the effects of propellers in the IVC and the SVC to help increase the pressure at the connector outlets [11]. A diagram of the propeller positions can be seen in Figure 5. The design utilizes two propellers connected to a central shaft to create an increase in pressure as the blood flows into the connector from the IVC and the SVC. The pressure increase was induced to be the same for both inlets to prevent back flow. This right ventricular device is designed such that the connector could be used with or without the propellers inserted into it, enabling the connector to have both an active and passive configuration. This way, if the inflow from the IVC and SVC openings of the connector were adequate to maintain healthy blood flow rates, the propeller would not need to be added. Conversely, if the flows into the connector are too weak, the propeller could be inserted to help increase the pressure at the outlets. The

current study is focused on the passive form of the connector, with the goal of optimizing the flow through it by identifying the proper combination of design variables corresponding to a particular age group.

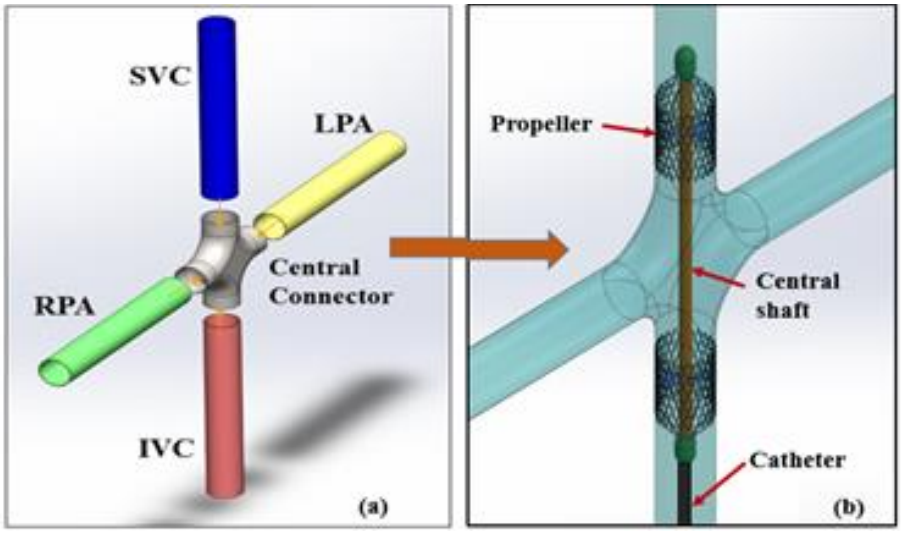

Figure 5. Connector and propeller configuration from *[11]*

1.2 Research Plan and Goals

The goal of this study is to find the optimal geometry and configuration for the passive flow portion of the connector. Optimization of the passive geometry of the connector could lead to more easily controlled flow interactions between the inferior and superior vena cava and the right and left pulmonary arteries as well as decrease the energy loss and blood damage. The previous study conducted by Jagani [8] found that the flared geometry exhibited superior hemodynamics compared to the other three configurations observed. The flared connector, as illustrated in Figure 4, created the most favorable combination of blood mixing, pressure variations and reduction in recirculation areas. Therefore, this flared configuration was selected as the basic for the geometric designs for this study. Additionally, taking inspiration from Soerensen et al [9] and Marsden et al. [10] , a flow diverter was also added to the central region of the connector in the second fold of this study to try to reduce blood damage, power loss, and recirculation. The overarching goal was to create a computational platform that could help identify an optimal configuration for the 4-way connector for each of the age groups suffering from right ventricular dysfunction, from neonates (age 1) up to the young adults (20 years of age). Another goal was to find out if the optimum ratio of opening radius to corner radius changed as the diameter and flow rates are changed (i.e. as the patient grows). If the optimal ratio stays the same, the optimal geometry for the connector can be found and scaled to fit any patient. However, if the optimal ratio changes with the flow rate and size of the arteries, patient specific connectors will have to be made. This would lead to the necessity of creating an easy to use program that would take in the dimensions of the IVC, SVC, LPA, RPA, and flow rate and find the optimal ratio for the connector.

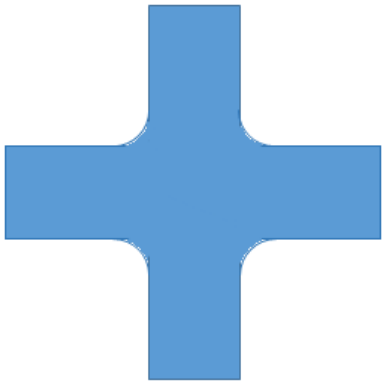

Figure 6. Flared Fontan cross section

1.2.1 Goals and objectives of the study

The goals of this thesis are to design an optimization method and guideline for creating TCPC connectors for patients between the ages of 1-20 suffering from single ventricle dysfunction. The individual overall goals are as follows:

- To use CFD to quantify the influences of connector parameters on power loss and blood damage estimates
- To create a guideline for patient specific optimized Fontan style TCPC connectors for ages 1-20
- To compare the benefits of adding a central diverter to the design of the connector for each of the different age groups
- To quantify Blood Damage Index and Power Loss in the observed optimized connectors

Chapter 2

2 Methodology

2.1 CFD Model

Models were created in ANSYS to effectively simulate the connector and capture the co-dependence between design variables. ANSYS uses an element-based finite volume method to discretize the objective geometry and provides second order accuracy in space and time. When solving the system, two numerical operations are conducted for each time step. The first operation involves linearizing the nonlinear equations and assembling them into the solution matrix to the generate coefficients. The second operation solves the linear equations using an Algebraic Multigrid method.

The models were run as Newtonian, steady state, laminar flow models. Table 1 shows parameters taken from the literature used to create the CFD models for this study. Table 5 shows the fluid properties used in this study. Newtonian flow was used based on the fact that the non-Newtonian behavior of blood is only significant for very low shear stresses (less than 0.15 Pa) *[13]*. While there would be some areas of low shear stress within the model, the vast majority of the model would exceed this minimum shear stress. Additionally, the assumption was made that the patients would be on blood thinning medications to prevent rejection of the device. These medications prevent the platelets in the blood from sticking together as well as increases the time need for clot formation. This change in the blood properties in addition to the findings of Merrill et. al *[14]*. This logic was also used by Wood et al. in their study of the medical physics of ventricular assist devices. Laminar conditions were assumed and justified by estimating the Reynolds numbers in each connector. The Reynolds numbers shown in Table 2 were approximated using the data from Table 1 and Table 5. All of the Reynolds numbers were found to be within the laminar range (less than 2100), justifying the assumption of laminar flow. Steady state simulations were performed for all the models considered. The pulsatile effects are neglected in the current study, to facilitate a quick design iteration and capture the co-dependence among all design variables and their effect on the objective functions. This assumption is often used in the design and development of ventricular assist devices, and is shown by Untaroiu et al. *[15, 16]* in their studies on blood damage and flow path designs for an artificial heart pump. Additionally, it is thought that the pulsatile effect in the right ventricle for a patient suffering from right ventricular dysfunction would be reduced, therefore, the assumption of steady state flow would

be well justified. Another assumption used in this study was that the orientation of the device was negligible, because the inertial term for the flow was relatively small.

Table 1: IVE, SVC, LPA, and RPA diameters *[17, 18]*, SVC flow rate *[19, 20, 21, 22, 23, 24]*, LPA and RPA pressures *[25, 26, 27]*, and Cardiac Output *[28]*

Age Group	LPA Diameter	RPA Diameter	IVC Diameter	SVC Diameter	Cardiac Output	SVC flow	LPA Pressure	RPA Pressure
(years)	(mm)	(mm)	(mm)	(mm)	(l/min)	(l/min)	(mm Hg)	(mm Hg)
1-5	8.75 - 11.43	8.38 - 10.5	4.4 - 7.54	4.1 - 7.26	1.4 - 3	1.1 - 1.6	11	11
6-10	12 - 13.97	11 - 12.64	8.64- 13	8.2- 12	3.1 - 4.0	1.75	11.5-13.5	11.5-13.5
11- 15	14.42 - 16.08	13 - 14.35	14.12 - 18.5	12.88 - 16.63	4.1 - 5	1.23-1.75	12-16	12-16
16-20	16.47 - 17.92	14.67 - 15.85	19.6 - 24	17.57 - 21.32	5 - 6	1.25-1.8	15-25(sys) 8-15(dia)	15-25(sys) 8-15(dia)

Table 2: Reynolds Number approximations for the IVC and SVC

Age Group	IVC Reynolds Number	SVC Reynolds Number
1-5	2003	1194
6-10	1888	1125
11-5	886	528
16-20	816	486

The age range from 1 to 20 was split into four different age groups (1-5, 6-10, 11-15, and 16-20 years) based on the collected parameters. A grid independence study was conducted on a geometry for the 11-15 age group connector to reduce the run time of the simulations while minimizing the grid's effect on the final results *[8]*. The final grid had a difference of less than 3% from the finest grid, with an element count of 115,572-440,744 depending on the size of the connector. Table 3 shows a general node and element count for each age group used in this study. Figure 8 shows an example of a completed mesh for the connector.

Table 3: Mesh characteristics for CFD analysis

Age group (years)	number of nodes	number of elements	min size (mm)
1-5	115572	312131	0.19572
6-10	115952	323034	0.20146
11-15	321509	1146003	0.21171
16-20	440744	1696350	0.20906

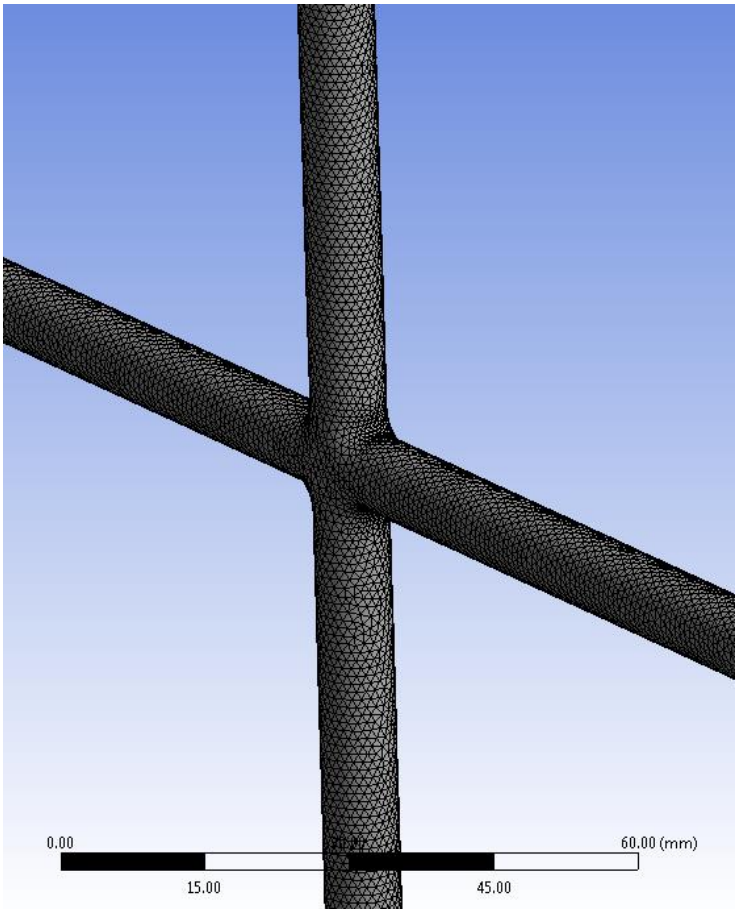

Figure 7. Visualization of the mesh for a right bypass connector

Equation (1 and (2 show, respectively, the mass and momentum conservation equations, which act as the governing equations for this study.

$$\frac{\partial \rho}{\partial t} + \frac{\partial}{\partial x_j}(\rho U_j) = 0 \qquad (1)$$

Where ρ is the density and U is the velocity vector.

$$\frac{\partial}{\partial t}(\rho U_i) + \frac{\partial}{\partial x_j}(\rho U_j U_i) = -\frac{\partial P}{\partial x_i} + \frac{\partial}{\partial x_j}\left(\mu_{eff}\left(\frac{\partial U_i}{\partial x_j} + \frac{\partial U_j}{\partial x_i}\right)\right) \qquad (2)$$

Where P is the pressure and μ_{eff} is the effective viscosity. Convergence was assumed at a normalized max residual less than $1e^{-4}$.

2.1.1 Boundary conditions and Blood Properties

Boundary conditions for the inlet flowrate, outlet pressure, and opening radius of the connector for each age group were found by averaging the values found in Table 1. Figure 8 show the designations of boundaries as they are referred to in this study. For age group 1-5, the opening radius was chosen to be 3.75 mm, the IVC flow rate was set to 0.03887 kg/s, SVC flowrate was set to 0.02385 kg/s, and the LPA and RPA pressures were set to 11 mmHg. For age group 6-10, the opening radius was chosen to be 6 mm, the IVC flowrate was set to be 0.06272 kg/s, SVC flow rate was set to 0.03092 kg/s, and LPA and RPA pressures were set to 12.5 mmHg. For the 11-15 age group, the opening radius was chosen to be 8 mm, the IVC flowrate was set to 0.08038 kg/s, the SVC flowrate was set to 0.02632 kg/s, and the LPA and RPA pressures were set to 14 mmHg. Finally, for the 16-20 age group, the opening radius was chosen to be 10 mm, the IVC flow rate was set to 0.09717 kg/s, the SVC flow rate was set to 0.02694 kg/s, and the LPA and RPA pressures were set to 15 mmHg. These values can also be found in .

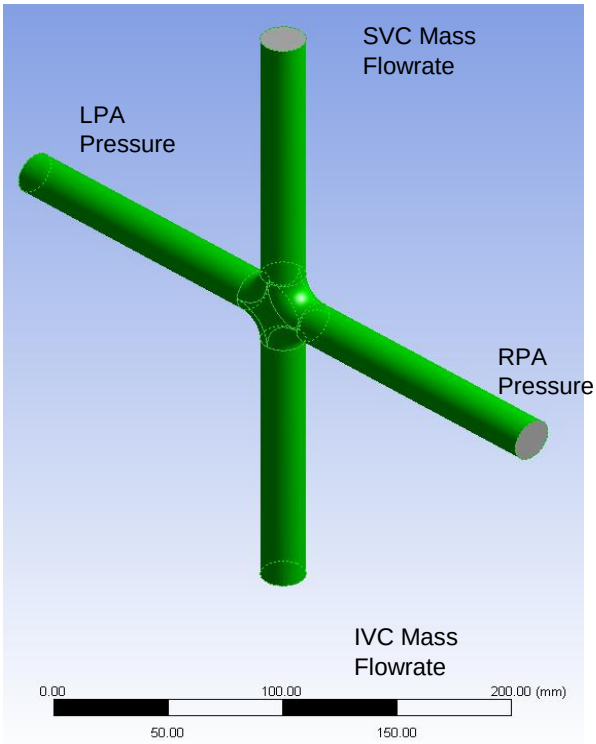

Figure 8. Computational Model. Illustration of boundary conditions for the model, green represents the walls of the model with Inlets at the top and bottom and outlets on the left and right.

Table **4**. This study was first conducted in *[29]* but was redone in this thesis using a more even spread of opening radii. The blood properties used to model the fluid in this study can be found in Table 5. The walls were modeled as no slip surfaces. The Blood Cell properties included were used for the Blood Damage Index calculation which will be explained in Section 2.3.

Table 4: Connector inlet and out let conditions based on age group

Age Group [years]	Opening Radius [mm]	ICV Mass Flowrate [kg/s]	SVC Mass Flowrate [kg/s]	LPA and RPA Pressure [mmHg]
1-5	3.75	0.03887	0.02385	11
6-10	6	0.06272	0.03092	12.5
11-15	8	0.08038	0.02632	14
16-20	10	0.09717	0.02694	15

Table 5: Simulation and blood properties

Property	**Value**
Blood:	
Molar Mass	64.458 (kg/mol)
Density	1060 (kg/m$^{3)}$
Dynamic Viscosity	0.003 (kg/ms)
Blood Cells:	
Molar Mass	67 (kg/mol)
Density	1094.1 (kg/m^3)
Diameter	0.0078 (mm)
Wall conditions	No slip

2.2 Design of Experiments and Optimization Algorithms

This program utilized a capability in ANSYS called design-of-experiments (DOE) to minimize power-loss and fluid particle residence time in connector to assists in estimation of blood damage index based on junction geometries. The chosen geometries were based on the relative size of the patient's arteries found in the literature. From this information, four DOEs were run using the average diameter for each group (diameters were assumed to be close enough to the same for the purposes of this experiment). The output variables used in these models were power loss and the average and maximum time for a particle to pass through the computational model. Time was used because of its direct connection to blood damage index. This was based on the idea that the longer a red blood cell takes to go through the connector, the more likely a recirculation or stagnation point has occurred [30, 31, 32, 33]. Power loss was calculated using Equation (3.

$$Power\ Loss\ (W) = A_{IVC} * v_{IVC} * p_{IVC} + A_{SVC} * v_{SVC} * p_{SVC} - A_{LPA} * v_{LPA} * p_{LPA} - A_{RPA} * v_{RPA} * p_{RPA} \quad (3)$$

Where A is the area, v is the velocity, p is the pressure and subtexts IVC, SVC, LPA and RPA indicate the variable's measurement location at the Inferior Vena Cava, Superior Vena Cava, Left Pulmonary Artery, and Right Pulmonary Artery, respectively [8]. The streamline capability in CFX-Post was used to calculate the average and maximum particle traversal times. A total of 100 streamlines were used for each model. The DOE set up for this study used the Enhanced Rotatable Central Composite Design capability. The Central Composite Design (CCD) finds the overall trends in the metamodel by creating a screening set of data points. This method is very efficient when running a DOE because it uses ANSYS' Optimal Space-Filling Design function; which finds the minimum number of points needed to run the optimization and maintain a good coverage for the response surface. This allows the DOE to be run more efficiently.

The Response Surface models for this study were created using Genetic Aggregation. The Genetic Aggregation response surface can be thought of as the weighted sum of the different response surfaces based on the metamodels. Equation (4 shows a mathematical representation of this method.

$$\hat{y}_{ens}(x) = \sum_{i=1}^{N_M} w_i * \hat{y}_i(x) \quad (4)$$

Where $\hat{y}_{ens}$ is the prediction of the aggregation, $\hat{y}_i$ is the prediction of the individual response surface, N_M is the number of metamodels used in the aggregation, and w_i is the weight factor for the individual response surface. For this method, the weight factor values are chosen to minimize the root mean square error between the points on the predicted aggregation and the cross-validation of the points found in the DOE [34].

The optimization used in this study utilized ANSYS's Multi-Objective Genetic Algorithm (MOGA) method with the objective functions set to minimize the power-loss and fluid residence time in the connector and effect constraints on these functions such that they would not fall below zero. This constraint was chosen because the set up does not add energy to the system so a value of negative power loss would be invalid. There are many multi-objective design optimization methods available that could have been used in this model. However, the majority of these methods fall into two categories; these include gradient based and non-gradient based methods. Gradient base methods require the functions and constraints to be differentiable. The non-gradient based methods can apply to non-differentiable problems. For example, genetic and evolutionary algorithms are non-gradient based, while the adjoint method is gradient based. Though genetic based algorithms are not as efficient as gradient-based algorithms, they are very robust and are well suited for complex and non-smooth problems. Additionally, they have been used frequently when dealing with problems in CFD [35]. The MOGA used in this study is a decision and evaluation algorithm that takes an initial population and generates new populations through processes called cross-over and mutation [36]. Cross-over is the process of combining two characteristics to get a different potentially better characteristic. Much like genes in biology can be combined to create new potentially better versions. Mutation is the alteration of one or more characteristics independent of cross-over to help prevent stagnation around a locally optimal result. This helps to ensure that the best overall outcome is achieved. The algorithm then updates the design points in the new population and validates the optimization for convergence. These steps are repeated until convergence occurs or the number of given iterations has been reached.

2.3 Blood Damage

As with any device being introduced into a patient's body, issues of rejection and blood damage must be addressed. Usually rejection is prevented through the use of medication that suppresses the body's immune response to the device, which can lead to some serious side effects for the patient. However, in addition to taking these side effects into account, devices that interact with the blood directly, issues regarding blood damage must also be looked into. Blood damage, especially when looking at an implantable device, is usually caused by hemolysis and thrombosis. Hemolysis refers to the wear and rupture of red blood cells. When the red blood cells rupture, they release hemoglobin into the surrounding fluid which can cause major health issues. Thrombosis is the formation of a blood clot within a venous structure. Clotting

occurs when the platelets in the blood are activated (change from a discoid shape to a more irregular shape with protrusions) and adhere to themselves and other particle within the vasculature (red blood cells, vessel wall, etc.) Clot formation within the vasculature can be extremely dangerous. The clot could hinder or stop blood flow through the affected area or, in some cases, the clot could break into smaller pieces and travel through the system to clog multiple places at once; either of these cases could result in a stroke or heart attack. To help reduce the likelihood and prevalence of hemolysis and thrombosis occurring within the connector, a blood damage estimation was incorporated in the DOE constraints and then calculated for the optimized connectors.

2.3.1 Blood damage modeling

The studies conducted in this thesis used CFD to simulate blood flow through the chosen connector geometries. As such, the blood cells were modeled as particles within the flow simulation. This allowed for the calculation of important stresses acing on the particles as they traveled through the model. Hemolysis and thrombosis are both related to the shear stresses acting on the blood. Hemolysis can occur when a red blood cell is exposed to either a small shear stress over long time, or a large shear stress over a short time. Large shear stresses within the blood flow can be found in areas of large velocity gradients. This can be seen either near the vessel walls or in areas of high vorticity. One the other hand, Thrombosis has been linked to instances where the shear stresses acting on the fluid is less than 1 Pa [37]. this can happen in recirculation areas or stagnation regions where the flow velocity is close to or at zero. Though there have been a many methods for quantifying blood damage, the most widely used scale is the blood damage index. The blood damage index (BDI) quantifies damage from hemolysis and thrombosis as it relates to shear stress and exposure time. This is why, for the DOE, traversal time through the connector was used as an estimate of BDI. Because exposure time is directly related to the BDI [33, 30, 31, 32], using the time in connector as an estimate for exposure time allowed for a basic estimation of the potential blood damage as well as saving on computational time. The actual BDI values for each of the connectors were calculated using the Lagrangian Method after the initial results of the optimization were obtained. The Lagrangian Method calculates the BDI of a particle by integrating the BDI of that particle at discrete points along its path. This was accomplished by tracking the blood cell particles as they passed through the connector. The equations used to calculate the BDI were based on the Scalar Shear Stress and the traversal time and can be found in Equations (5 thru (7 [41].

$$\text{Scalar Shear Stress} = \sqrt{\frac{1}{6}\left[\sum\left(\sigma_{ii} - \sigma_{jj}\right)^2 + 6\sum\tau_{ij}^2\right]} \tag{5}$$

Where σ and τ are stress components defined by i = x, y ,z, j= x, y, z, and i ≠j.

$$\Delta(\text{BDI})_i = C\,a\left[\sum_{j=1}^{i}\tau(t_j)^{\frac{b}{a}}\,\Delta t_j + D(t_0)\right]^{a-1}\tau(t_i)^{\frac{b}{a}}\,\Delta t_i \tag{6}$$

$$\mathrm{BDI} = \sum_{i}^{N} C\, a \left[\sum_{j=1}^{i} \tau(t_j)^{\frac{b}{a}} \Delta t_j + D(t_0) \right]^{a-1} \tau(t_i)^{\frac{b}{a}} \Delta t_i \qquad (7)$$

Where *C*, *a*, and *b* are the experimentally obtained constants found in Table 6 and *t* is time. These values were then averaged over all of the particles to obtain the average BDI for the system.

Table 6. Power Law Equations Constants developed by Giersiepen et al. *[41]* Heuser and Opitz et al. *[42]* and Zhang et al. *[37]*

	Range				
	Shear Stress	Exposure Time			
Model	(Pa)	(msec)	C	a	b
GW	< 255	< 700	3.62×10^{-5}	0.7850	2.416
HO	< 700	< 700	1.8×10^{-6}	0.750	1.991
TZ	$50 - 320$	< 1500	1.228×10^{-5}	0.6606	1.9918

Chapter 3

3 Optimization of the connector geometry

The first study conducted for this thesis was to optimize the flared configuration of the connector given a specific opening radius and opening conditions. As stated in Chapter 2 the optimization process used for this study was a Multi-Objective Genetic Algorithm. Using a DOE in combination with an optimization process can allow for a more comprehensive study of trends in the connectors. For example, using the response surface, local sensitivity graphs can be produced that show how each of the output functions vary with changes in the parameters. In the case of this study, the parameter that varied was the corner radius of the connector, and the output functions used for the optimization process were minimization of average and maximum time in the connector and power loss.

3.1.1 CFD Set up

Four DOEs, one for each age group, were run to complete this part of the study. Each DOE took in the inlet and out let conditions and opening radius given in Table 4 from Chapter 2 as well as a range of diameters for the connector corner radius. For each age group the corner radius was varied between just larger than the opening radius, to about three times the opening radius. The specific ranges for the four groups were 3.8-12, 6.5-19.5, 8.5-25.5, and 10.5-31.5 respectively. The corner radius could not be modeled any smaller than the opening radius due to geometrical constraints. The upper bound on the range was chosen to be about three times the radius to help ensure that the outer limits of the design were accounted for in the DOE. The boundary conditions for each of the age groups were as shown in Chapter 2 in Table 4. The material properties used in the modeling can also be found in Chapter 2 Table 5. Additionally, to avoid unrealistic results, the power loss was constrained to be positive. A negative power loss would indicate that the connector was adding power to the flow, which would be impossible. Similar constraints were added to the average and maximum time in connector parameters. The DOE, results surface model, and optimization were set up as stated in Chapter 2, using an enhanced rotatable central composite design for the DOE, genetic aggregation for the response surface model, and MOGA for the optimization. For all age groups, a baseline model was created with corner radius 25% larger than the radius. This size was intended to reflect an estimate of a sutured joint based on the idea that when vessels are sutured together there will be a slight flare at the junction.

3.2 Results and Discussion

Through this optimization process, it was confirmed that as the patient's age and artery size change, the optimal size and shape of the connector also changes. Each DOE solved the model for 9 separate corner radii. These points were then analyzed using the Genetic Aggregation Response Surface function, which gave a response surface with an average R^2 value above 0.9, indicating that the response surfaces are good representations of the models. Specific R^2 values for the models can be found in Table 7 and a plot of the predicted values verse the observed values from the design points of one of the age groups can be found in Figure 9. From Figure 9 we see that the points match very well with the one to one ratio line, meaning that the predicted values are close to the observed values.

Table 7: R^2 values for Response Surface Results

Age group	Power Loss R^2	Average Time R^2	Max Time R^2
1-5	0.99964	0.98921	1
6-10	0.99542	0.96329	0.99859
11-15	0.99241	0.96562	1
16-20	1	1	1

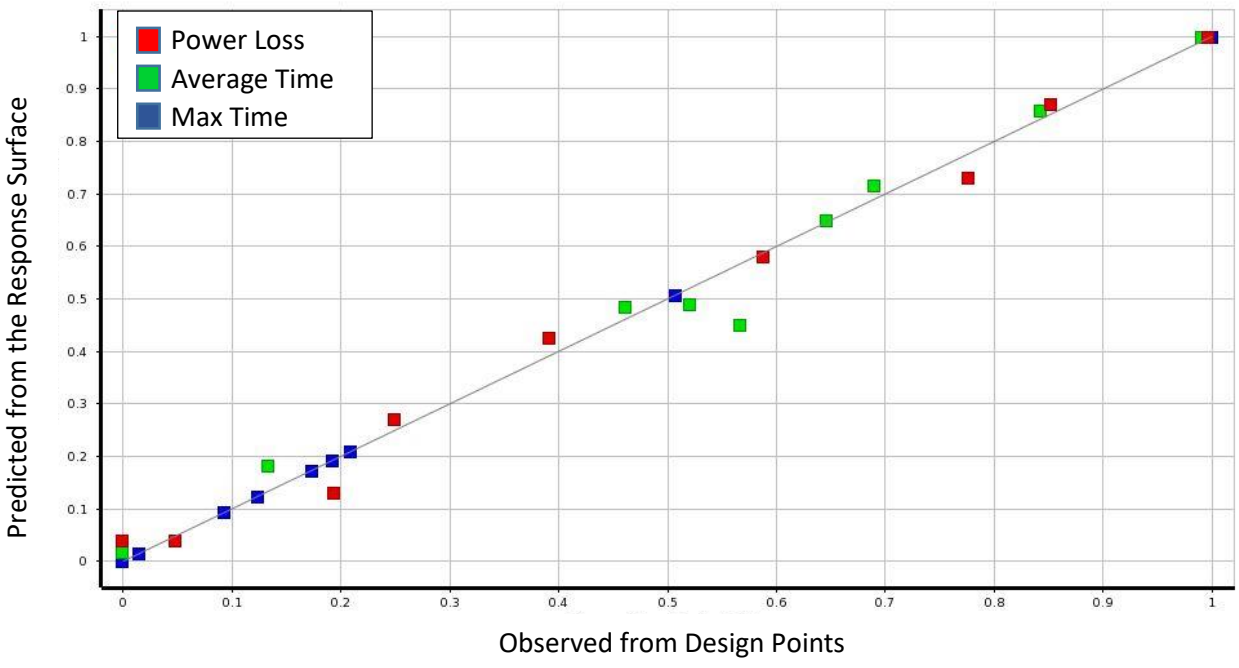

Figure 9. Predicted results vs. Observed results for output variables from design points for the 11-15 age group. All of the points are very close to the one to one ratio line, showing that this is a good representation of the model.

The response surfaces for each of the output parameters can be seen in Figure 10 thru Figure 12. The trends in these Figures are reflected in the sensitivity bar graphs shown in Figure 13. All of these Figures show a decreasing trend in power loss and an increasing trend in average time in connector for increasing corner radius size. The max time output did not have a well-defined relationship with the corner radius size. This was expected because the max time would be affected by the recirculation areas in the connector, thereby making this measurement less consistent than the other two output values. However, the fact that the power loss and average time in the connector had a consistent relationship with the corner radius through all four age groups lends a certain amount of validity to the results and can aid in interpreting the individual results from the four optimizations.

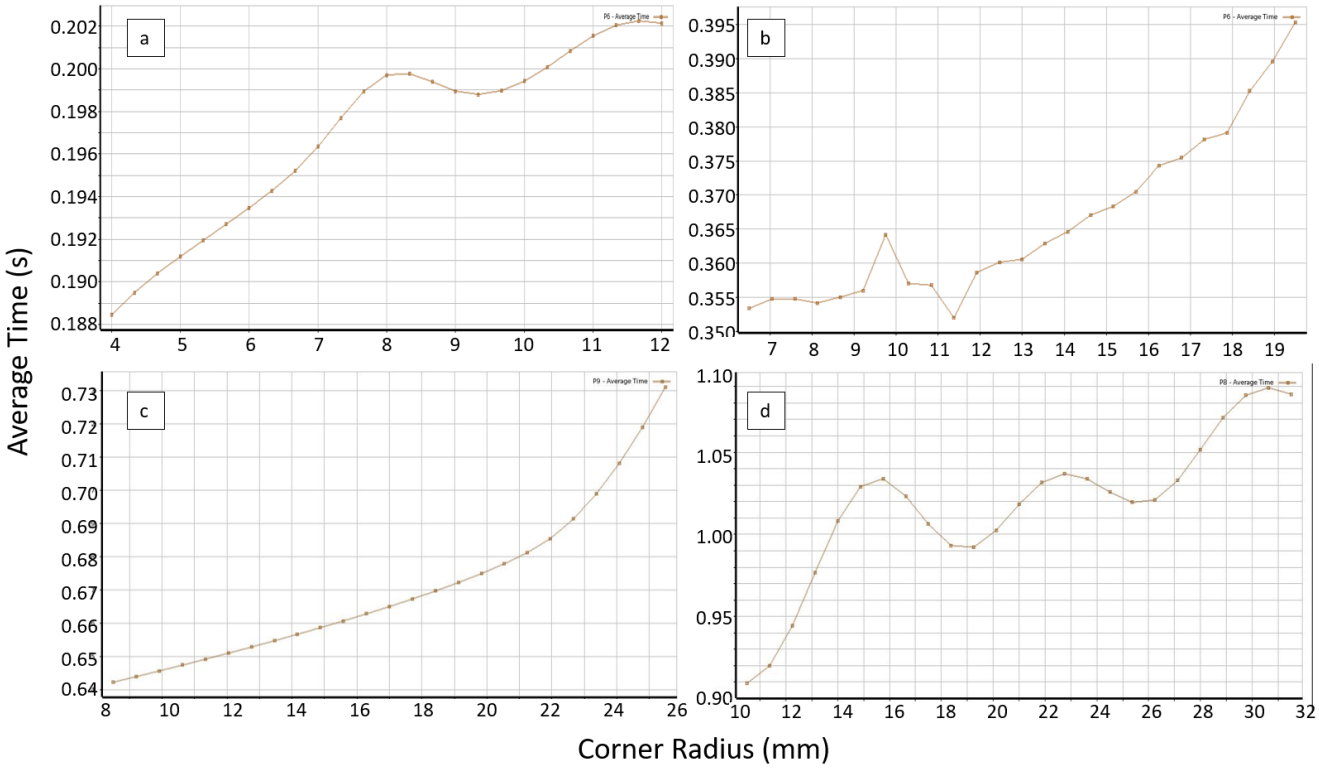

Figure 10: Average time response curves for age groups (a) 1-5, (b) 6-10, (c) 11-15, and (d) 16-20.

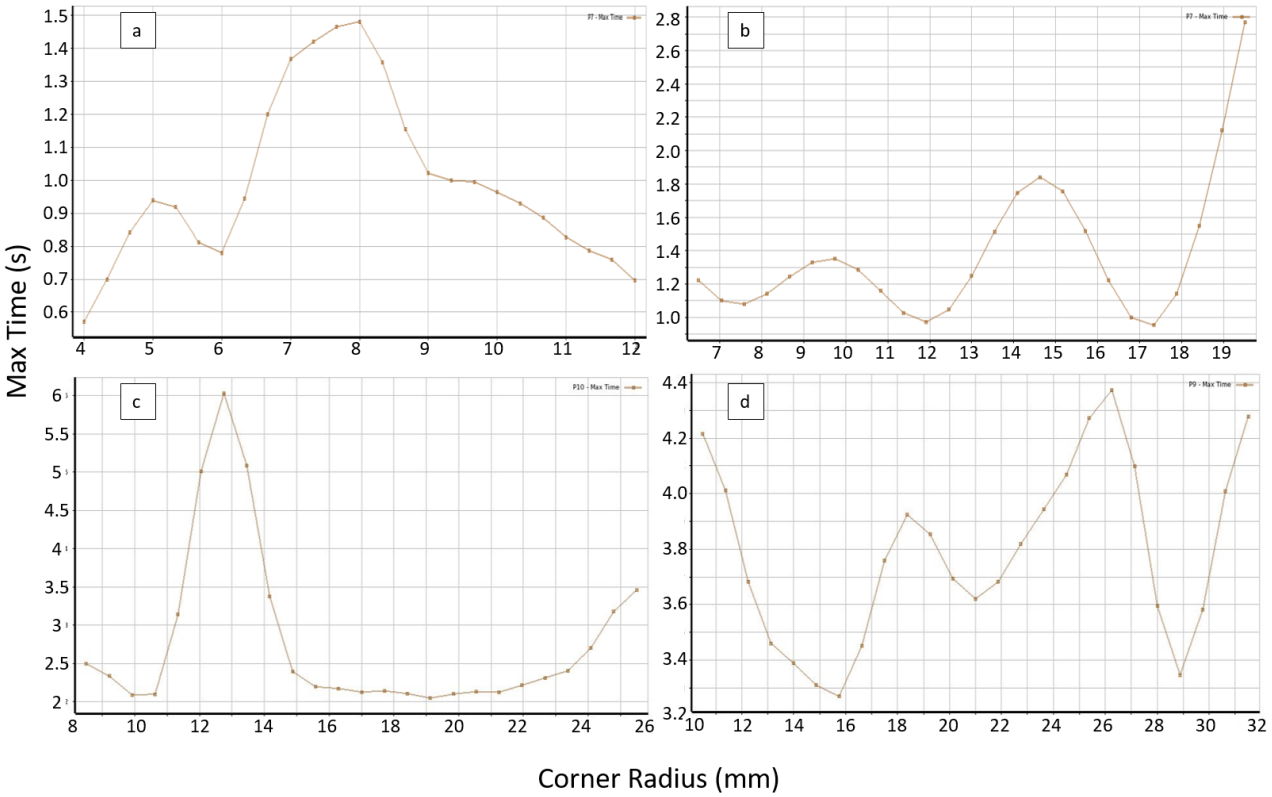

Figure 11: Max time response curves for age groups (a) 1-5, (b) 6-10, (c) 11-15, and (d) 16-20.

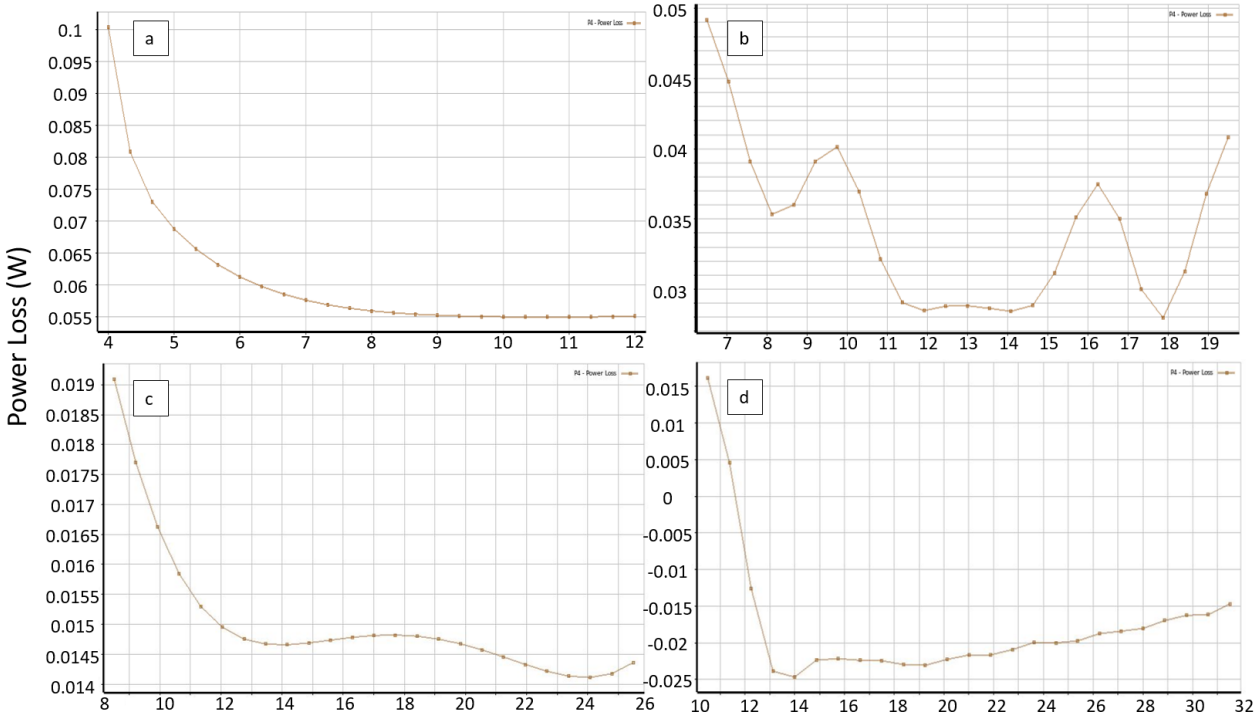

Figure 12: Power loss response curves for age groups (a) 1-5, (b) 6-10, (c) 11-15, and (d) 16-20.

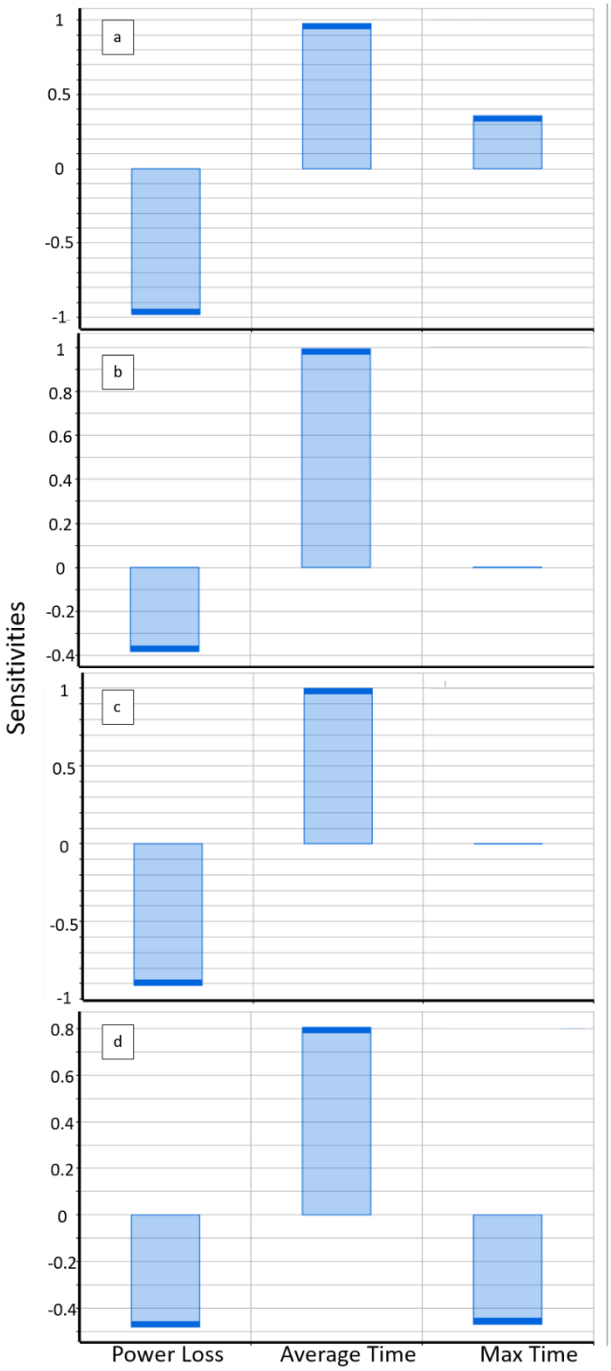

Figure 13: Output sensitivity for age groups (a) 1-5, (b) 6-10, (c) 11-15, and (d) 16-20.

After generating the response curves, a MOGA was run to find three appropriately optimized "Candidate Points" or corner radii geometries. The data for these points from each of the age groups can be found in Table 8. One optimized geometry was chosen from these points for each age group based on a comparison of the output parameters, the response surface curves, and a visual comparison of the velocity and pressure contours. An example of which can be seen in Figure 14. In this case, the geometry corresponding to the 20.475 mm corner radius was found to give the best balance of favorable output conditions and reduced recirculation areas (areas of low or zero velocity). The configurations chosen for each age group can be found in Table 9. Figure 15 shows the values from Table 9 plotted by output value.

Table 8*:* Parameter values of candidate points separated by age group

Age Group	Corner Radius	Power loss (W)	Average Time (s)	Max Time (s)	Opening : Corner
1-5					
Opening Radius (mm): 3.75	4.36	0.079788	0.18957	0.71120	0.860
	5.24	0.066368	0.19173	0.93677	0.716
	5.88	0.061838	0.19319	0.77079	0.638
6-10					
Opening Radius (mm): 6	11.430	0.028889	0.35239	1.0172	0.525
	12.132	0.028602	0.35944	0.98463	0.495
	13.585	0.028618	0.35944	1.5363	0.442
11-15					
Opening Radius (mm): 8	10.625	0.011837	0.63048	2.8394	0.753
	15.215	0.011749	0.64036	4.2412	0.526
	17.255	0.011486	0.66538	5.1421	0.464
16-20					
Opening Radius (mm): 10	13.185	0.008902	0.9031	3.1393	0.758
	15.645	0.008418	0.9059	2.8727	0.639
	20.475	0.007745	0.9473	3.9586	0.488

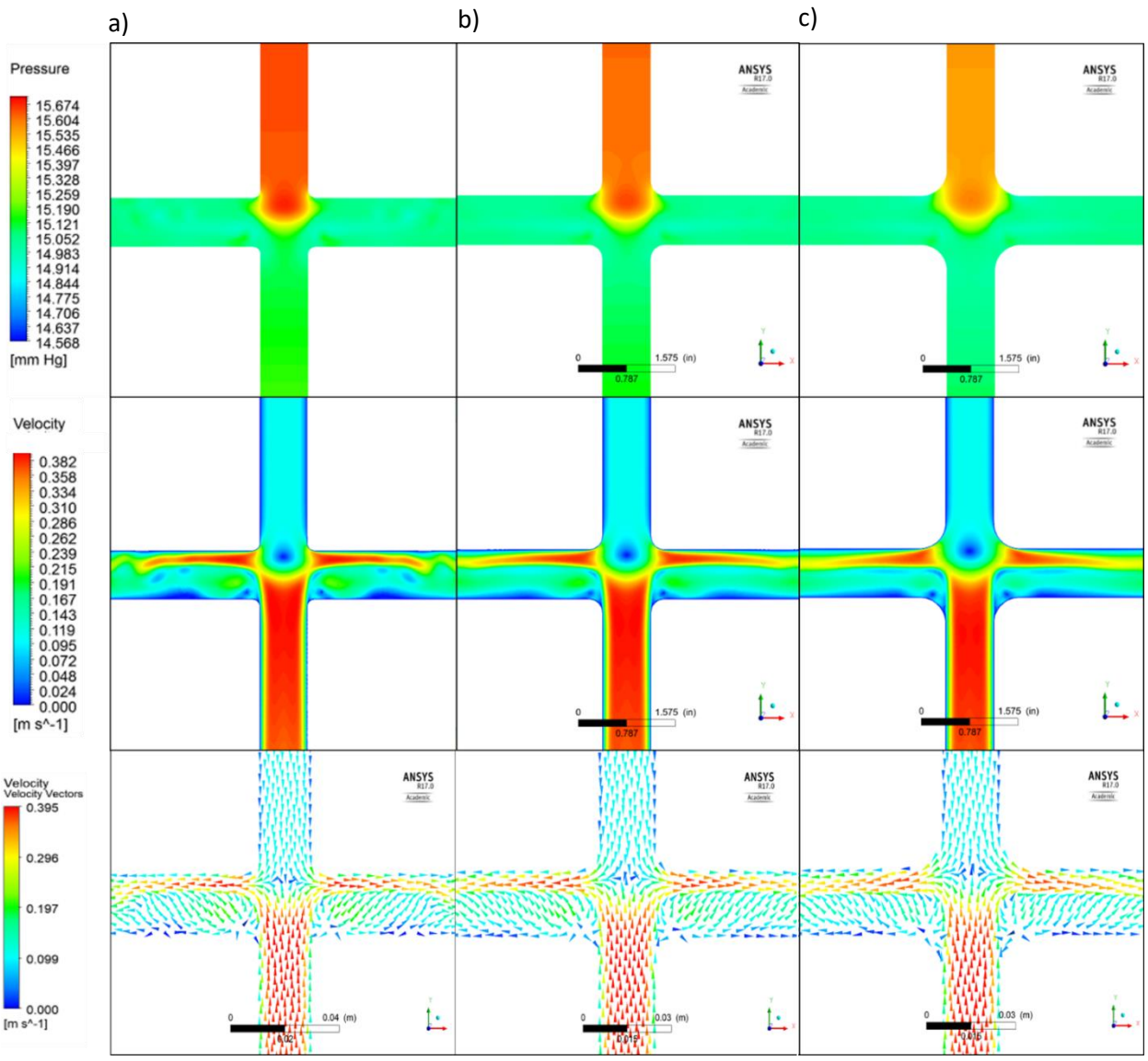

Figure 14. Velocity (bottom) and Pressure (top) contours for the 3 of the candidate points candidate points for the 16-20 age group in order from largest corner radius to smallest

Table 9: Optimized geometry parameters for the four age groups

Age group	Corner Radius	Power Loss (W)	Average Time (s)	Max Time (s)	Opening :Corner
1-5	5.88	0.061838	0.19319	0.77079	0.638
6-10	11.430	0.028889	0.35239	1.0172	0.525
11-15	15.215	0.011749	0.64036	4.2412	0.526
16-20	20.475	0.007745	0.9473	3.9586	0.488

From Figure 15, the trends in the opening to corner radius ratio, power loss, and maximum and average time in the connector can be seen. A slightly decreasing trend can be seen in the opening to corner radius ratio, indicating that as the opening radius (and associated flowrate and pressure) increase the optimal corner radius needs to increase as well. This is probably to help accommodated for the increased mass flow through the inlets of the connector. Power loss shows a defined decreasing trend, indicating that as the parameters of the connector increase the power loss in the connector is reduced. This may be a result of the decrease in the wall surface area to volume ratio as the opening and corner radii increase. Because of the way the connector is shaped, the major sources of loss is from the jet collision at the center of the connector and the losses from wall shear stress. Therefore, as the wall surface area to volume ratio decreases the comparative losses in power due to this shear stress also decrease. The maximum and average traversal time in the connector both show increasing trends as the opening radius increases. This is most likely due to an increase the overall size of the connector as well as in the recirculation area sizes as the junction space at the center of the connector increases in volume.

Table 10: Optimized geometry parameters for the four age groups

Age group	Corner Radius		Power Loss (W)		Average Time (s)		Max Time (s)	
	Optimized	Baseline	Optimized	Baseline	Optimized	Baseline	Optimized	Baseline
1-5	5.88	4.6875	0.061838	0.080438	0.19319	0.19371	0.77079	0.81828
6-10	11.430	7.5	0.028889	0.036305	0.35239	0.35052	1.0172	1.64131
11-15	15.215	10	0.011749	0.012026	0.64036	0.62596	4.2412	2.26686
16-20	20.475	12.5	0.007745	0.009004	0.94727	0.89510	3.9586	3.1592

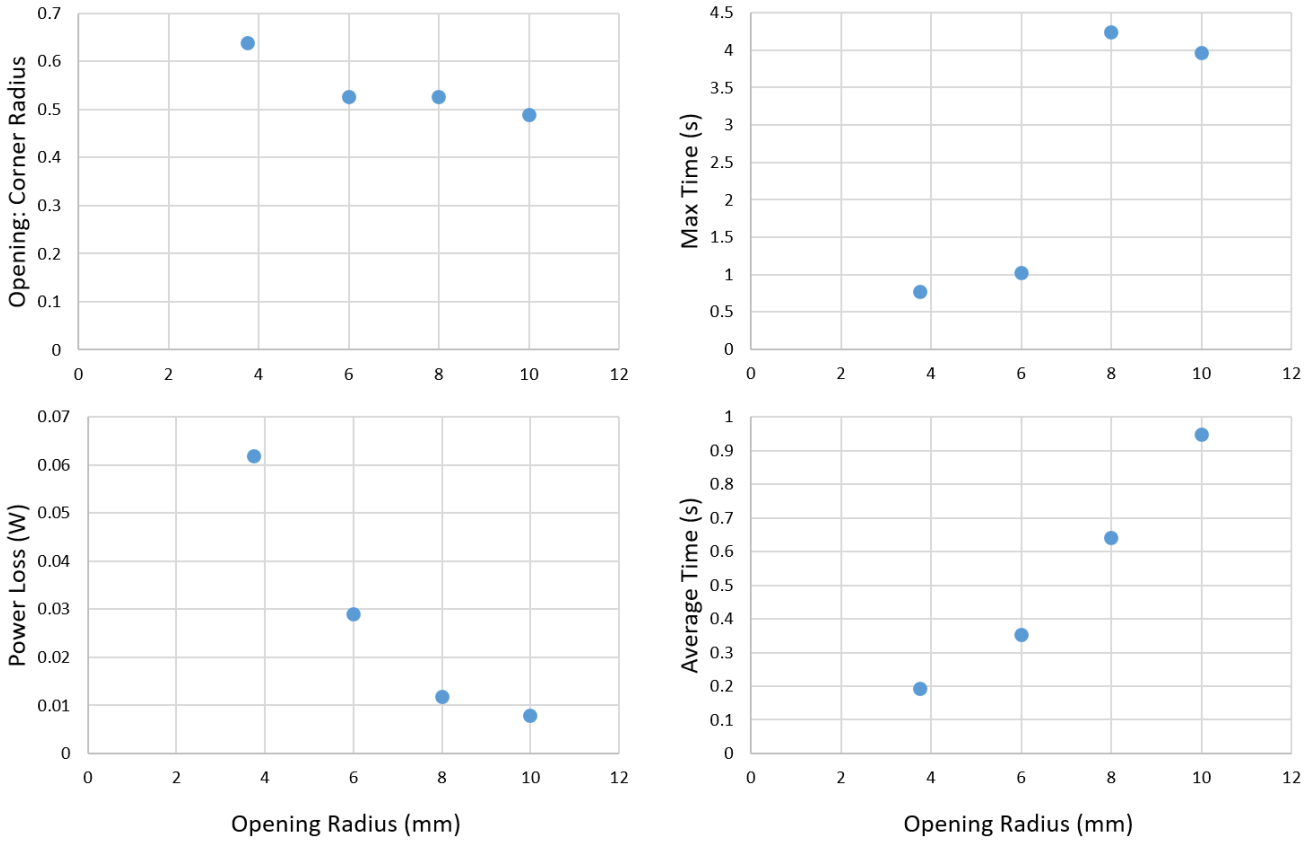

Figure 15: Plotted output values for the optimized geometries for each of the age groups

A comparison of the base line to optimized model continues the trends found in Figure 10 to Figure 13. The optimized connector for each case had a larger corner radius than the baseline connector, thus showing a decrease in power loss and an increase in the average time as per the previously stated trends. However, looking at the contours of the optimized model compared to the baseline, the larger corner radius of the optimized connector creates a less drastic pressure change and a more organized flow path than the baseline connector. Figure 16 thru Figure 20 show example comparisons of the streamlines, pressure and velocity contours, and vorticity for the baseline and the optimized models. In Figure 17, it can be seen that the streamlines for the optimized connector achieve straight paths more quickly than the baseline. This I likely do to the more gradual introduction of the flow from the IVC and SVC into the junction. In the pressure contour comparison in Figure 16 the pressure spike near the SVC side of the central junction is

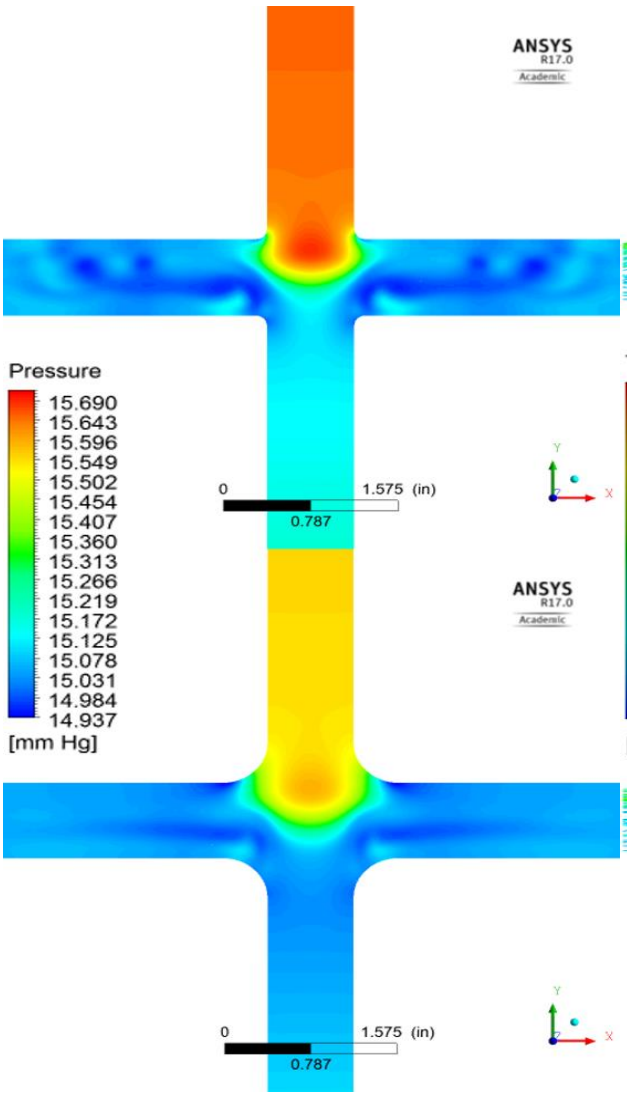

Figure 16. Pressure contour comparison between (top) baseline and (bottom) optimized models.

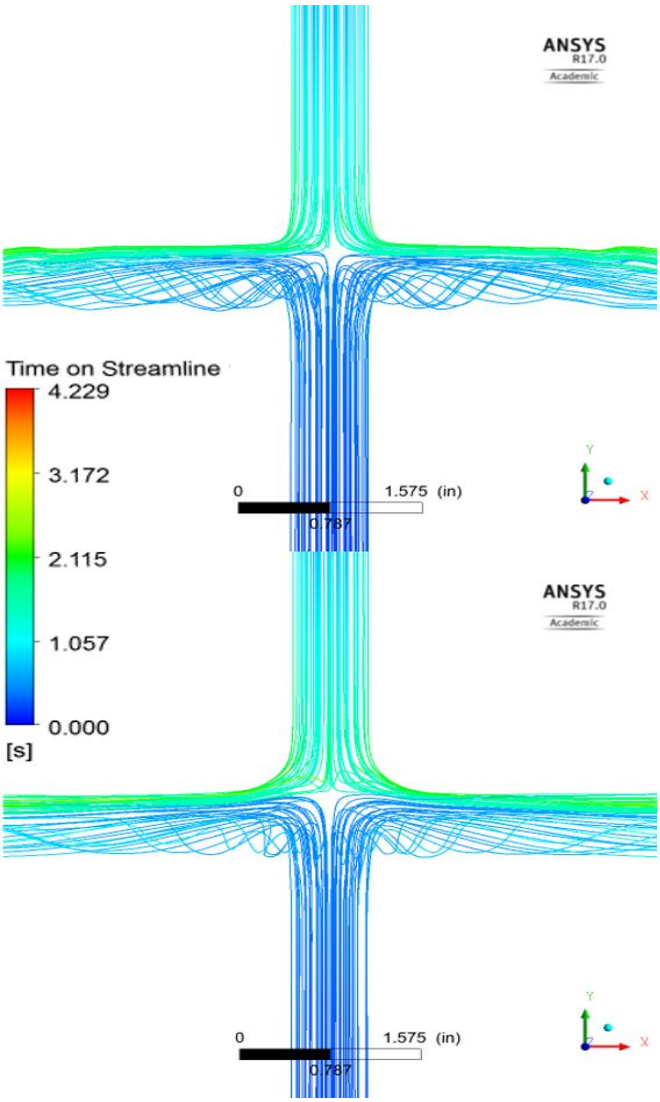

Figure 17. Streamline comparison between (top) baseline and (bottom) optimized models.

noticeably reduced in the optimized connector. This reduction is most likely due to the reduction in connector junction volume. In Figure 18, the velocity contours mirror what is seen in both the streamline and pressure contour comparisons, the flow appears more uniform and ordered in the optimized connector than in the baseline. Additionally, there is a reduction in the flow stagnation areas (areas of dark blue) along the lower edges of the LPA and RPA portions of the connector in the optimized model compared to the baseline. These stagnation areas can be better seen in the velocity vectors shown in Figure 19. This is also likely due to the more gradual introduction of the IVC and SVC flows to the central junction. Figure 20 shows the Q-Criterion vortex core region with coloring according to the region's vorticity (taken as the curl of the velocity flow) of this area of stagnation and recirculation. Again, through the optimized model's reduced vortex core regions, the comparison shows that the optimized model has a straighter. This more organized flow is likely the reason for the reduction in power loss for connectors with a larger corner radius. All of these observations show that the optimized connector is, indeed, superior to this study's baseline.

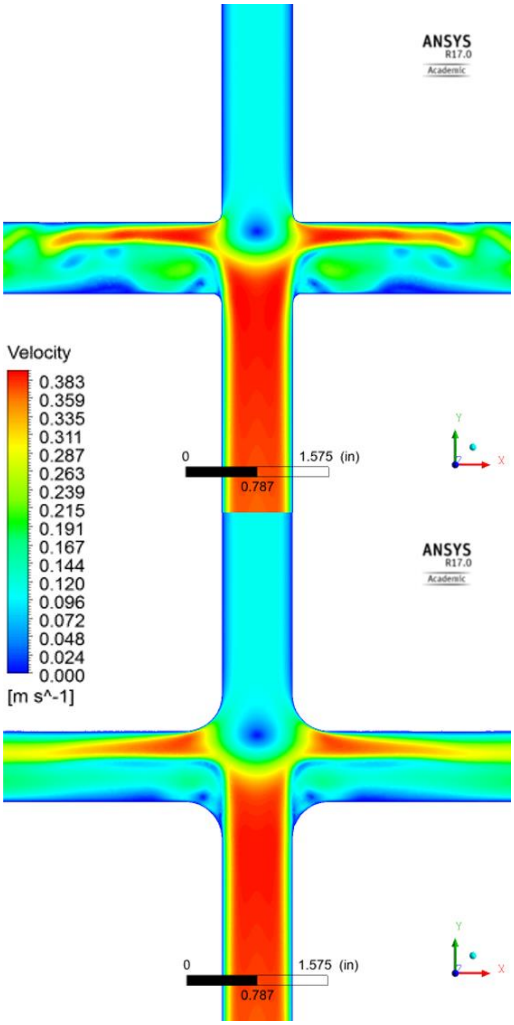

Figure 18. Velocity contour comparison between (top) baseline and (bottom) optimized models

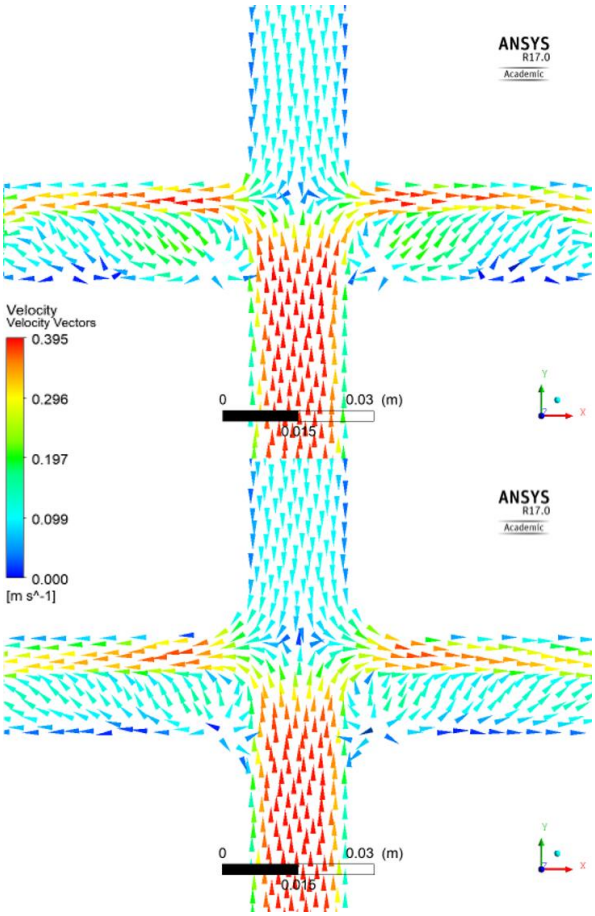

Figure 19. Velocity vector comparison between (top) baseline and (bottom) optimized models

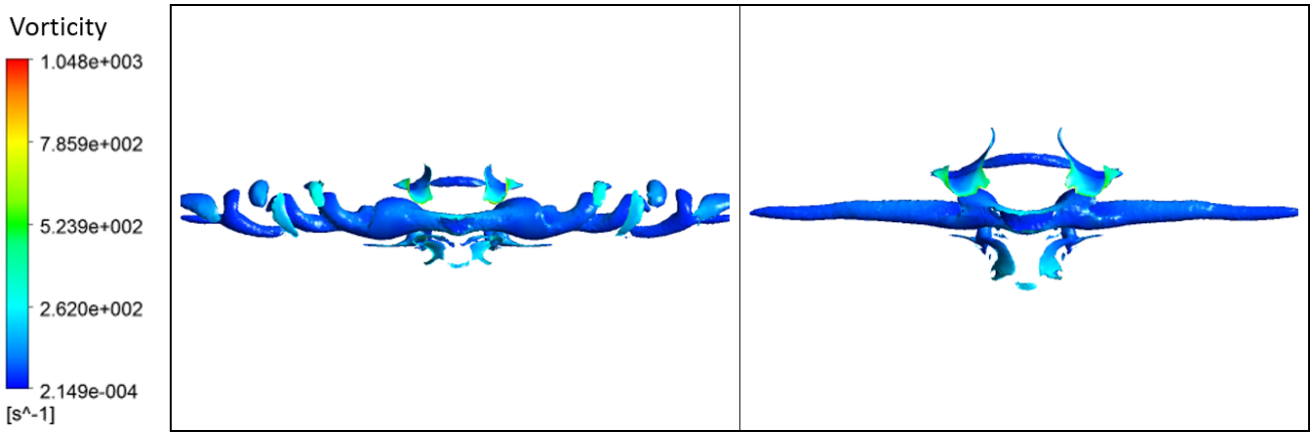

Figure 20. Q-Criterion vortex core region with vorticity contour coloring for (left) baseline and (right) Optimized models

3.3 Conclusion of geometry optimization

This study focused on optimizing the passive geometry of a four-way connector that could be used to improve the Fontan procedure by regulating the blood flow through the junction of IVC, SVC, LPA, and RPA. Based off of previous research conducted by Jagani et al [8], a flared geometry was selected and optimized for minimum energy loss and blood damage propensity (blood damage index estimated by residence time of a fluid particle passing through the connector) for four age groups spanning 1 to 20 years of age. The study was conducted using a 3-D model in ANSYS-CFX for various corner radii.

It was found that the optimal geometry of the connector does change with opening radius, and in fact shows a slightly decreasing trend with increasing opening radius. This was made evident by comparing the ratios of the Opening to Corner radii for each of the four age groups. In addition to this finding, a trend of decreasing power loss and increasing average time in model was found as the opening radius was increased. However, some persistent problems occurred in all of the connector in this study. Because the flows from the IVC and SVC are in direct opposition from each other, a recirculation area will always be present at the point of collision for the two flows. This recirculation area is especially dangerous because it is located at the stagnation point of the flow collision. Stagnation regions in blood flows encourage thrombosis, or the clotting of the blood. Typically, clots or other arterial buildup first start to form on the inner walls of a vessel and are usually only considered dangerous when they become big enough to break off and travel through the blood stream. Should a clot form in the stagnation region at the flow collision in the center of the connector, it would already be free to travel through the bloodstream, potentially leading to stroke, heart attack, and maybe death. Therefore, it is important to try to reduce or, negate this central recirculation region. To do this the idea of a central diverter was conceptualized and implemented to improve the optimized connectors explored here. The following chapter will discuss how the diverter was implemented and optimized.

Chapter 4

4 Addition of a Flow Diverter

This section focuses on the optimization of a central flow diverter to supplement the optimization from the previous chapter. Again, as stated in Chapter 2, the optimization process used utilized results from a DOE of the diverter geometries, varied by several key parameters, to implement the Multi-Objective Genetic Algorithm method. At conception, the addition of the diverter was thought to potentially reduce or negate the central recirculation region found in all of the geometries for the connector. Thus reducing the likelihood of thrombosis and floating clot formation. Additionally, because of the nature of the diverter, it was thought that the flow paths through the connector would become smoother, allowing for potentially shorter average blood cell traversal time through the connector.

4.1 CFD set up

Just as in the previous study, four DOEs, one for each age group, were run to find the optimal geometry for the diverter. For each DOE, the settings and geometry for the optimized connector for the given age group was used as the base. The diverter was then created by removing the center portion of the baseline connector and replacing it with a geometry that directed the flow around where the central recirculation area had previously been. An example of this can be seen in Figure 21.

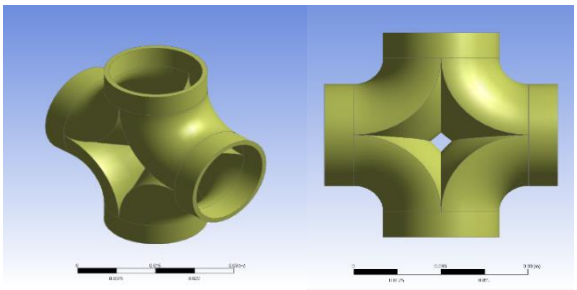

Figure 21: 3D image of the connector with a flow diverter

The idea is similar to what both Marsden et al [10] and Soerensen et al [9] studied. However, rather than basing the geometry on branches which could ultimately enlarge the cross-sectional area and overall size of the connector, the central diverter geometry was configured to take up just as much room as the optimized connector from the Chapter 3. Additionally, the diverter to set up to have independent curve profiles for the IVC and SVC diverter sections. Thus allowing for an asymmetric placement of the diverter to help account for the difference in inlet flowrate between the IVC and SVC. The parameters used for the DOE process in this case governed the sweep profiles of the IVC and SVC portions of the diverter. The spline functionality of the profiles allowed for independent alteration of the depth and curvature shape of the profile for the IVC and SVC diverter sections. The definition parameters for these profiles can be seen in Figure 22 and the values and ranges used for these parameters can be found in Table 11.

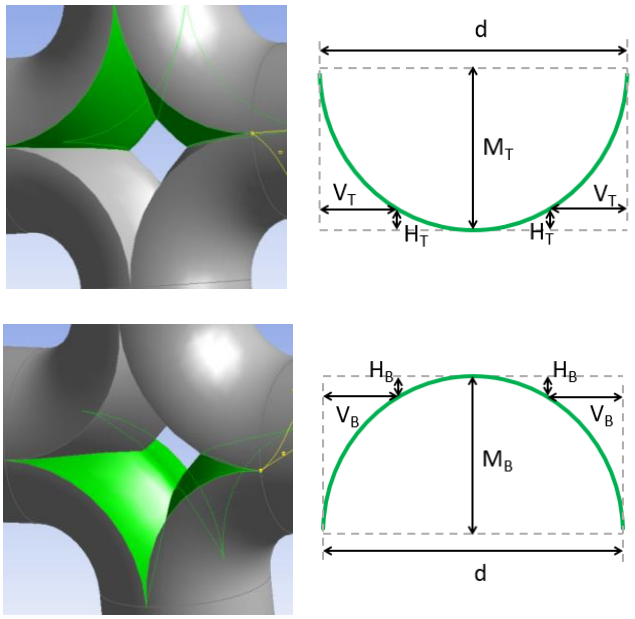

Figure 22: (Top) top and (Bottom) bottom profiles (right) and sweeps (left) that control the shape of the flow diverter

Table 11: Parameters for Baseline Model and Diverter Profiles

Parameter	Description	Age group			
		1-5	6-10	11-15	16-20
d	Opening Diameter (mm)	7.5	12	16	20
M_T	Top Profile Center Height (mm)	1.75-3.75	3-6	3-8	3-10
H_T	Top Profile Curve Adjustment –Height (mm)	0.5-1.75	1-3	1-3	1-3
V_T	Top Profile Curve Adjustment – width (mm)	2-3.5	2-5.5	2-7	2-9
M_B	Bottom Profile Center Height (mm)	1.75-3.5	3-6	3-8	3-10
H_B	Bottom Profile Curve Adjustment -Height(mm)	0.5-1.75	1-3	1-3	1-3
V_B	Bottom Profile Curve Adjustment – width (mm)	2-3.5	2-5.5	2-7	2-9

4.1.1 Optimization parameters

The equations for power loss and the procedure used to find average and maximum time in connector were the same used in Chapter 3 for the initial optimization study. However, because of the increase in varying parameters (from 1 to 6), each DOE ran closer to 90 design points for this study. To reiterate from Chapter 2, for each design point, the DOE ran a new configuration of the model. This includes generating a new geometry, meshing that geometry, and solving the system. The Enhanced Rotatable Central Composite Design was used for this DOE process as well. This process sets a number of screening data points to best find and use the overall trends in the metamodel, which aids the Optimal Space-Filling Design function in selecting the smallest number of points on which to run the analysis to get the best coverage for the response surface. By finding the smallest number of points to calculate, the function makes the DOE more efficient.

Again, similar to the previous optimization, a Genetic Aggregation was run on the data that was collected. The resulting R^2 values associated with the output functions, which can be seen in Table 12 were found to be sufficiently high to ensure the accuracy of the analysis. This is also reflected in the goodness of fit plot shown in Figure 23. The Multi-Objective Genetic Algorithm (MOGA) method was also used, with constraints such that the objective functions do not fall below zero.

Table 12: R^2 values for Response Surface Results

Age group	Power Loss R^2	Average Time R^2	Max Time R^2
1-5	1	1	0.9943
6-10	0.99397	0.98417	0.99193
11-15	1	0.97309	0.96977
16-20	0.99958	0.97381	0.94062

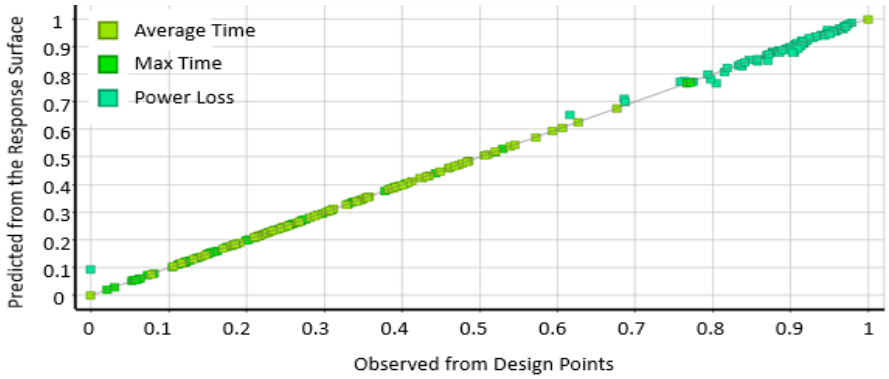

Figure 23: Goodness of fit plot for Predicted vs. Observed values

4.2 Results and Discussion

There are some apparent trends in the actual geometry of the connector. After conducting the optimization process sensitivity curves were generated to show the dependence of the output variables on the input parameters. The sensitivity curves seen in Figure 24 show only the sensitivities for the middle profiles lengths for the top (M_T) and bottom (M_B) profiles because these were found to have the most effect on the

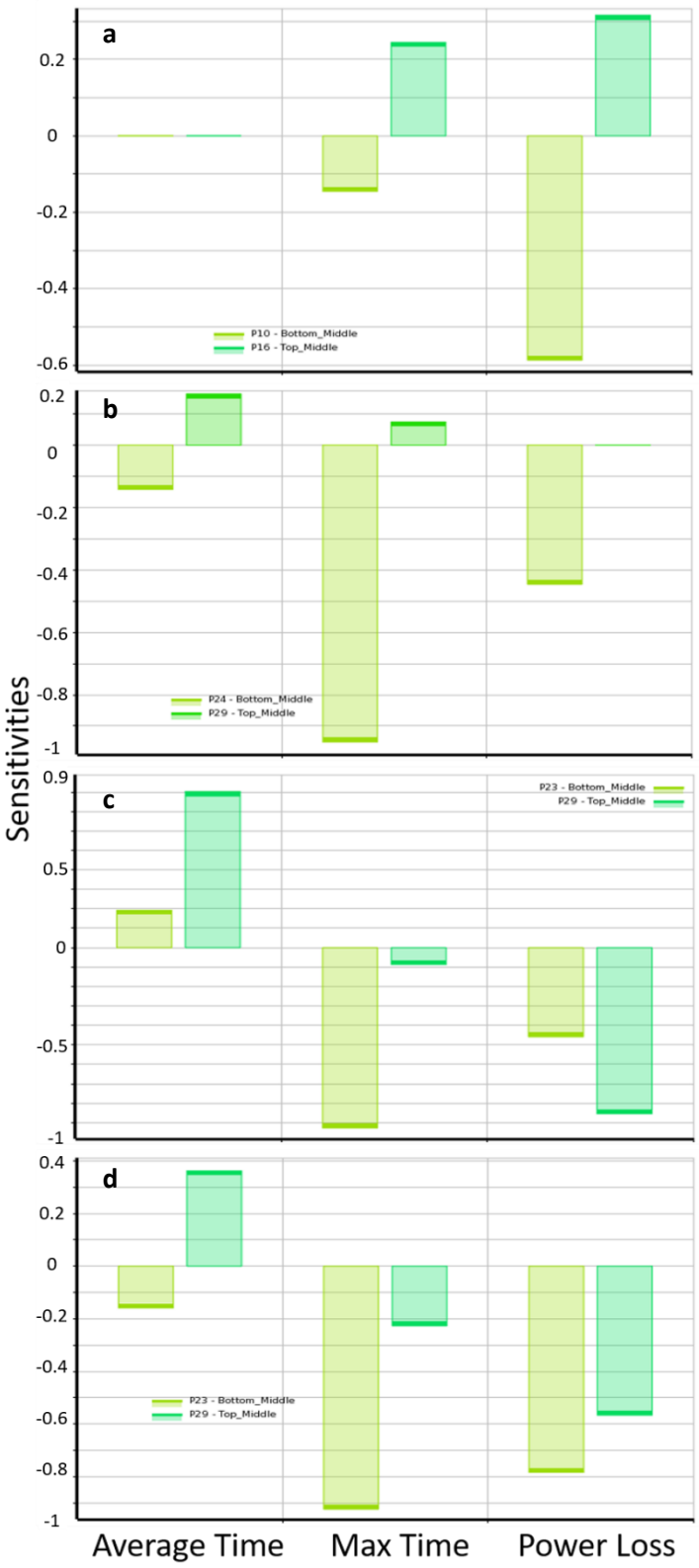

Figure 24: Sensitivity Curves for age groups a) 1-5, b) 6-10, c) 11-15, and d) 16-20.

size of the central diverter. Additionally, the other parameters' effects on the shape of the diverter are largely interdependent; meaning that how one parameter effects the shape depends on the value of the other parameters. So, while this aided in observing all of the possible profile shapes, the sensitivity for these parameters are too interconnected for the sensitivities to give a good idea for the individual parameter's effect on the diverter overall. However, just looking at the two middle length parameters for the diverter can lead to some interesting observations. For example, it can be seen that power loss had a consistent negative sensitivity to M_B. This means that power loss would typically decrease with increasing M_B. A similar trend was seen between M_B and max time. Average time seemed to be the lease affected by M_B showing a small, inconsistent sensitivity to M_B. This shows that typically a larger M_B will result in a more efficient connector. Moving on to M_T, an interesting trend can be seen across the age groups. As the age group increases from 1-5 to 16-20, the sensitivity of the Mas Time and Power Loss output variables changes from a positive (increases with increasing M_T) to a negative (decreases with increasing M_T) relationship, though the sensitivity of Max Time on M_T was very small. This shows a shift in either the trending geometry or flow rate ratio between the IVC and SVC as the age groups progress from 1-5 to 16-20 and could prove important for future studies on this topic.

Table 13: Objective value comparison between the baseline model (BL), optimized model (OP), and the optimized model with a flow diverter (OPwD)

Age group	Power Loss (W)			Average Time (s)			Max Time (s)		
	OPwD	OP	BL	OPwD	OP	BL	OPwD	OP	BL
1-5	0.0044782	0.061838	0.080438	0.28175	0.19319	0.19371	0.6526	0.77079	0.81828
6-10	0.0016945	0.028889	0.036305	0.51625	0.35239	0.35052	1.2943	1.0172	1.64131
11-15	0.00022926	0.011749	0.012026	0.9477	0.64036	0.62596	2.765	4.2412	2.26686
16-20	0.0010522	0.007745	0.009004	1.3245	0.94727	0.89510	4.298	3.9586	3.1592

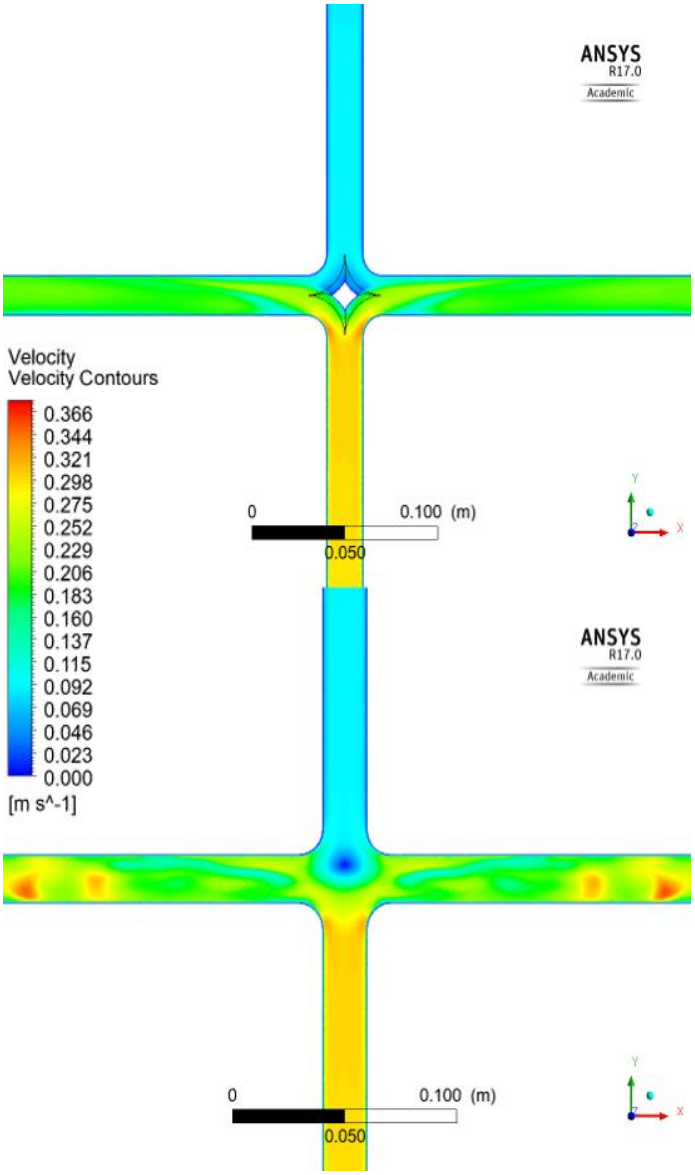

Figure 26: Velocity comparison between the optimized (bottom) and optimized with a diverter (top) models

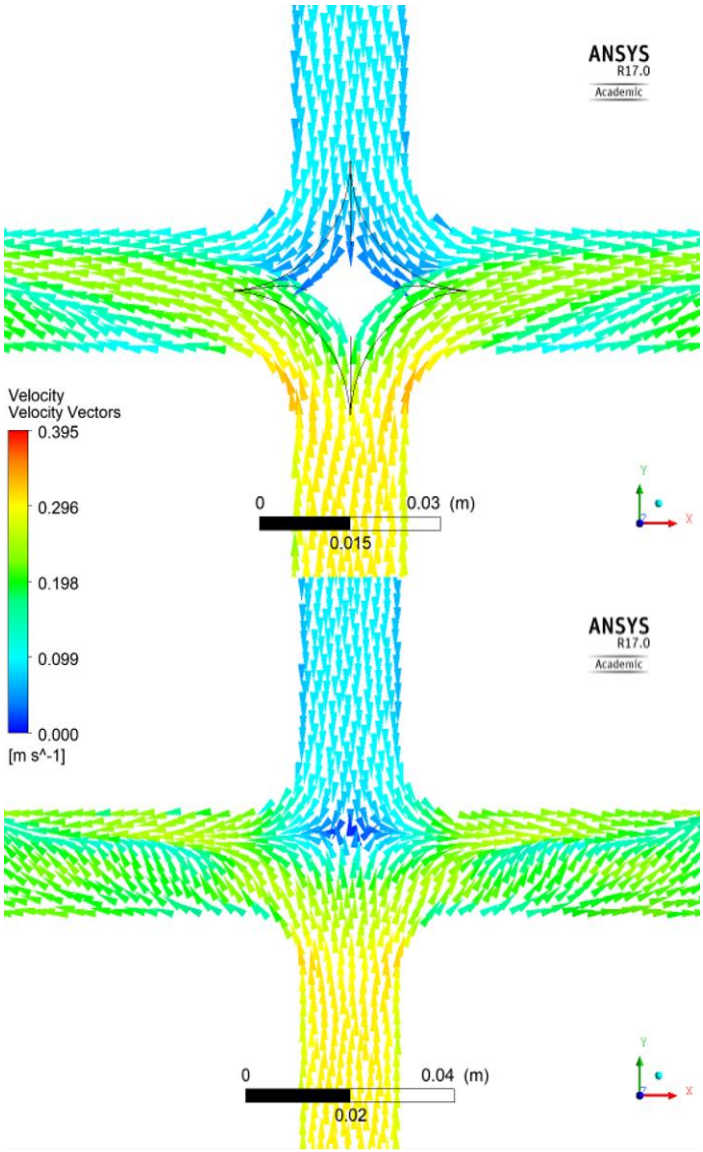

Figure 25. Velocity vectors for the (bottom) optimized and (top) optimized with a diverter models

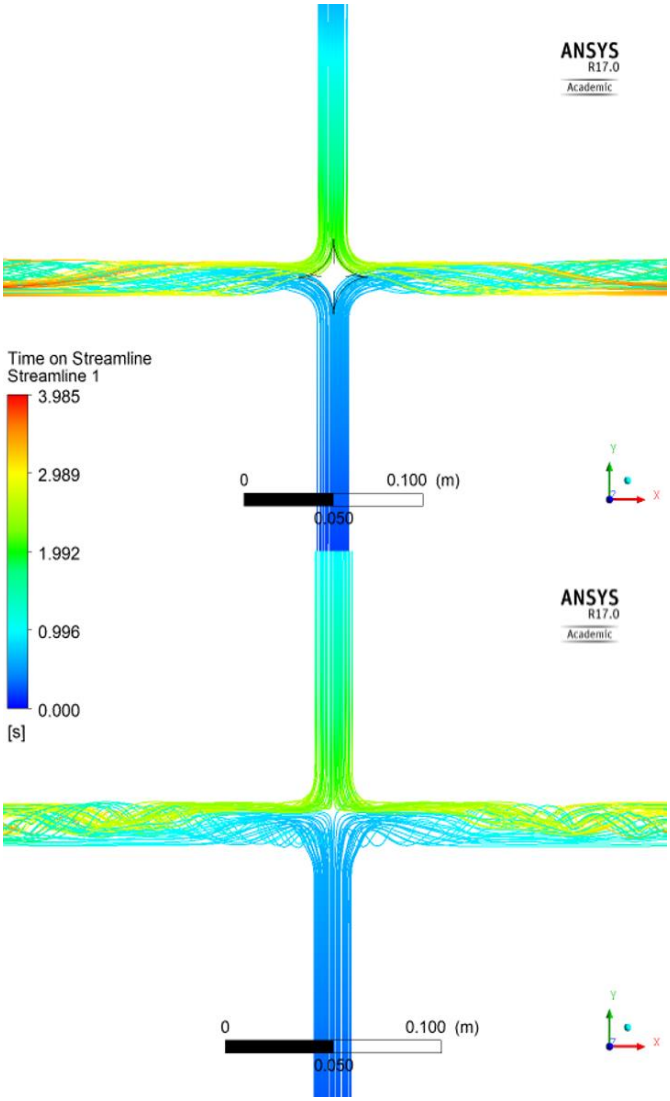

Figure 27: Comparison of Velocity Contours for the Baseline Model (left) and the optimized Symmetric Diverter (right)

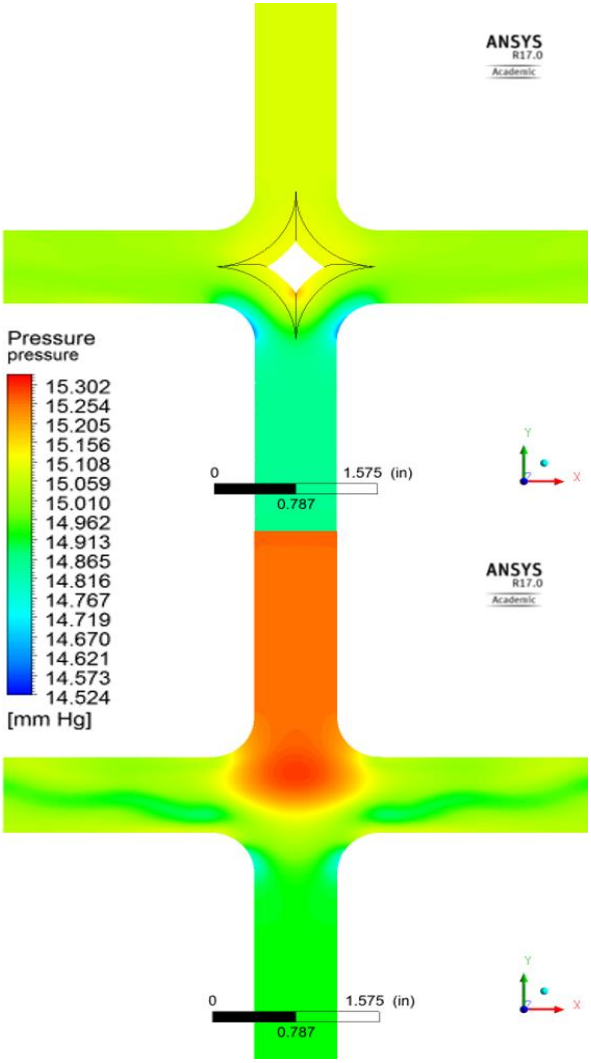

Figure 28: Pressure Contours for the Baseline Model (Left) and the Optimized Symmetric Diverter (Right)

The other numerical results of this study, also seen in Table 13, show an improvement in power loss for the optimized connector with a diverter compared to both the optimized and baseline models from the previous study. However, the diverter models consistently had longer average and maximum times in the connector. This is most likely due to the "no-slip" boundary condition introduced when adding the diverter itself. This means that the velocity at the wall of the diverter will be zero and will also enforce the viscus effect near the wall, potentially leading to an overall slowing of the flow through the connector. While the diverter did reduce the stagnation and recirculation are in the center of the connector junction, the fact that the diverter was made up of stationary no slip walls would have added extra drag to the flow, potentially increasing overall time in the connector. Fortunately, a look at Figure 26 and Figure ***25*** will show an almost complete negation of the central recirculation and stagnation point in the model with the diverter compared to the optimized model. This means that the increase in time in connector is not due to the creation of a new or enlarged stagnation or recirculation region in the diverter model. On the contrary, looking at the velocity contours in Figure 26 and the streamlines in Figure 27, the flow for the diverter model seems to

show improved flow organization and more controlled mixing between the IVC and SVC sourced blood. This can also be seen in the vertex core comparison seen in Figure 29. The vortex cores in this region were calculated using the Q-Criterion method and colored based on the vorticity of the area, where vorticity was taken to be the curl of velocity. From this Figure, the reduction in the vertex core regions for the optimized compared to the baseline, and the optimized with diverter compared to the optimized can be clearly seen. Vertexes could cause losses within the connector as well as create small stagnation areas. Thereby increasing the likelihood of clot formation. This decrease in vertex core regions seen in Figure 29 as the models progress from baseline to optimized with a diverter shows that the optimized with diverter geometry is an improvement over the baseline and optimized geometries.

The trend of continued improvement in the diverter model is continued when looking at the pressure contours. The comparison between the diverter model and optimized model pressure contours, seen in Figure 28, shows a far better pressure differential in the case with the diverter than the optimized. This is most likely because the collision between the two inflows does not occur in the diverter case. For the optimized connector without the diverter, the flows from the IVC and SVC collide in the connector junction. However, the point of collision is based on the difference between the flowrates of the two sources. Because the IVC has a larger flow rate than the SVC, the collision point is pushed more towards the SVC junction opening causing a pressure build up in that section of the connector. The diverter helps to alleviate this pressure build up by splitting and redirecting the flow from the IVC and SVC into the LPA and RPA at a set point within the junction.

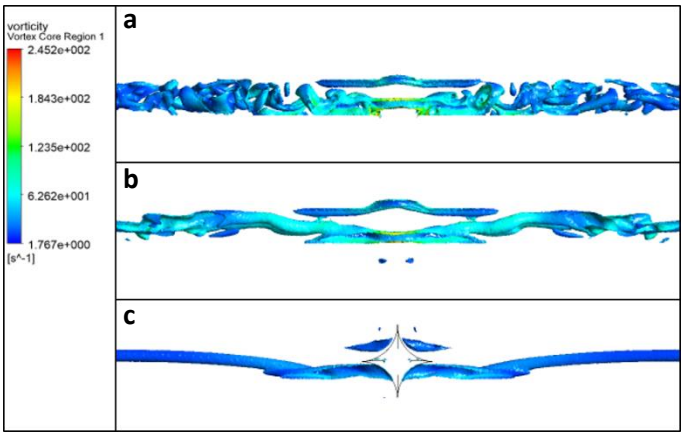

Figure 29: Q-Criterion Vortex Core region comparison between the a) baseline, b) optimized, and c) optimized with a diverter

The final comparison between these geometries was their effect on the Blood Damage Index for the flow. For this and Chapter 3's studies, traversal time through the connector was used as an estimate of the Blood Damage Index (BDI) in the DOE to save computational time and because it has a direct relationship to the BDI [33, 30, 31, 32]. Average and maximum times were calculated using the same streamline settings in CFX-post mentioned in Chapter 2. Also as stated in Chapter 2, the actual BDI for the connector was to be calculated after the initial results of the optimization using the Lagrangian Method, which calculates the BDI of a particle by integrating the instantaneous BDI of that particle at discrete points along its path. The BDI values for the baseline, optimized, and optimized with diverter geometries can be seen in the first category column in Table 14.

Table 14: Blood damage index values for the baseline, optimized, and optimized with diverter models for the TCPC connector

Age Group	Baseline		Optimized		Optimized with Diverter	
	IVC	SVC	IVC	SVC	IVC	SVC
1-5	1.06E-05	1.20E-05	6.44E-06	7.63E-06	4.34E-06	4.09E-06
6-10	8.41E-04	6.36E-04	5.53E-04	5.54E-04	1.95E-04	6.72E-04
11-15	6.10E-05	6.10E-05	4.32E-05	7.76E-05	1.23E-05	2.06E-04
16-20	3.25E-05	7.87E-06	1.94E-05	5.83E-05	1.90E-05	4.50E-05

These values show a decreasing trend in BDI for the IVC sourced blood as the columns progress from the baseline to the optimized with diverter geometries. However, there is also an increasing trend in BDI for the SVC sourced blood for this same progression. Though there is higher flow rate through the IVC than the SVC, which could lead to the argument that a decrease in the IVC sourced BDI is more influential than the increase in SVC sourced blood, this increase in SVC BDI should still be considered. A closer inspection of the SVC BDI values shows that in most cases, the optimized SVC value was very close to the baseline, but showed a larger increase for the optimized with diverter geometry. This could be because of the limitations of the diverter geometry for a fixed connector corner radius. In most of the cases, the diverter was found to have an optimal placement around where the recirculation point occurred. Though the diverter does help to stabilize the flow interaction between the two inlet flows and better direct those flows to the LPA and RPA, the actual location, size, and shape of the diverter may have been a compromise between optimal top and bottom diverter geometries. When looking at the sensitivity values from Figure 24, it can be seen that the M_B parameter had a larger effect on the output values than the M_T parameter. This means that a change in the M_B parameter would cause more of an effect in the output values than the same change in the M_T parameter, leading to the possibility of the optimization finding a more favorable geometry for the IVC (bottom) half of the diverter at the expense of the SVC (top) half of the geometry. Though this did lead to lower values for the overall power loss in the connector as well as a decrease, in some cases a drastic decrease, in the IVC BDI, it would be best to be able to optimize both the IVC and SVC portions of the diverter without having to make these concessions.

4.3 Conclusions

The focus of the study conducted in this chapter was to improve the geometries of the optimized four-way connectors found in Chapter 3 by adding a flow diverter to negate the persistent central recirculation region. Using a baseline model optimized through previous studies [29, 11, 8], a DOE was conducted to optimize the geometry of a central flow diverter to minimize power loss and BDI. The study was conducted using a 3D model in ANSYS-CFX for varying the upper and lower diverter curvatures. Through this study, it was found that the addition of the flow diverter into the connector did greatly decrease power loss and overall BDI. In addition to reducing the area and intensity of the central recirculation region, the new geometry with the diverter decreased the BDI for the blood from the IVC. However, the BDI for the SVC sourced blood increased for the optimized with diverter geometry. This was most likely because of the larger influence of the IVC portion of the diverter on the output values than the SVC portion. Though this did result in a decrease in power loss and IVC BDI as well as a reduction in the stagnation and recirculation regions within the connector, further development of an optimization design to take into account the interference between the IVC and SVC portions of the diverter would be ideal. However, the overall results show that the addition of a diverter is a valuable contribution of the overall connector geometry.

Chapter 5

5 Closing statements

5.1 Conclusions

Currently, the most common surgical procedure used to correct right ventricle dysfunction is the Fontan procedure. This procedure sutures the Inferior Vena Cava (IVC) and the Superior Vena Cava (SVC) directly to the Left and Right Pulmonary Arteries (LPA and RPA, respectively), bypassing the right ventricle. To improve this procedure, a Total Cavopulmonary Connector (TCPC) was created. This would allow for a consistent junction between the IVC, SVC, LPA, and RPA. The focus of this study was optimizing the TCPC connector explored in previous studies by Jagani et al and myself. The goal was to find geometric characteristics that had direct effects on power loss and average and maximum time in the connector.

For the first part of the study, the only geometric parameter that was varied was the corner radius size. This resulted in the discovery of a slight decreasing trend in power loss and increasing trend in average time in the connector for increasing corner radius. Additionally, as the opening radius (and associated flowrate and pressure boundary conditions) increased, there was a very slight decrease in opening to corner radius ratio. This is an important trend because it shows that there is a direct relationship between the optimal corner radius and the opening radius and associated conditions, which could lead to the development of a more intuitive guide system for creating patient specific connectors.

The second part of the study attempted to reduce or negate the central recirculation area that persisted through both the baseline and optimized models from the first study. The overall results showed a decrease in power loss as well as a reduction in the BDI for the IVC sourced blood, but an increase in the average and maximum time in the connector and the BDI for the SVC sourced blood. It is thought that the increase in the average and maximum time could be due to an overall slowing of the flow at the diverter due to the additional wall friction forces, and the increase in the SVC BDI could have occurred due to a compromise in the positioning of the diverter. However, the decrease in power loss, the reduction of the central recirculation area, and the smoothing of the flow paths in the diverter geometry compared to the baseline and optimized models show that while not perfect, the diverter is an improvement to the geometry of the connector.

The trends found in this study are a good starting point to creating a guideline for patient specific connectors. However, there are still some trends that need to be studied before this guideline can be created. Future studies on this topic could look into the trends relating the size of and flowrate through the arteries to the age. Then combining those trends with the results in this thesis, it would be possible to create a patient specific guide or modeling program that could find the optimal geometry for the connector based on the patient's age.

5.2 Future Works

The final goal of this research is to create a platform that could take in information from an MRI and 3D print a fully optimized patent specific connector. The results obtained in this study show the first steps in this direction and provided some valuable observations. Potential future works to continue this research would be to conduct experimental testing on these geometries. While a test rig was previously created to measure the flow characteristics of a connector with a dual propeller, the system was not sensitive enough to accurately measure the small differences in these characteristics for the connector alone. Preliminary experimental results obtained this way showed power loss very close to zero but with large fluctuations in the ICV, SVC, LPA, and RPA pressures as well as outlet flows that were too large compared to the inlet flow. The fluctuations in pressure could have been caused by air leakages in the system. The offset between the flowrates was most likely due to the use of two vastly different flow measurement device for the inflow and outflow monitoring system. The inflow flowrates were taken using Transonic H11XL flow sensors, which indirectly measure the flowrate, while the out flow flowrates were taken using Digiten FL-308T flow meters, which measure the flowrate directly. While these inconsistencies may have been negligible when measuring the larger pressure and flow difference seen in the presence of a dual propeller, the fluctuations in the pressure measurements and the offset between the flowrate values were too great for accurate and confident power loss calculations when measuring the connector alone. For future studies, an overhaul of the test rig should be completed to reduce any extraneous losses in the system and ensure precise and accurate measurements of the flow characteristics.

Another future step would be to explore the use of a transitional turbulence model instead of a laminar model. It was found that by using the laminar flow setting for the models, the presence of the central recirculation area as well as the very nature of the colliding inflows from the IVS and the SVC created some more complicated flows which may not have been fully represented in the laminar case solution. This issue could potentially be overcome by changing the flow type from laminar to mixed flow, or transitional-turbulence flow model, at least for the connector without a diverter. This would allow for a more accurate quantification of the small turbulent areas within the connector. Thus increasing the accuracy of the simulation.

In addition to the suggestions mentioned above, future studies into this topic could benefit from combining the corner optimization and the diverter optimization into a single DOE. In the case of this thesis, the optimizations were run separately to see if the addition of a diverter would improve the results of the optimized connector. Now that the results are known , a study that finds the optimal combination of corner radius and diverter size for each age group could be helpful and may show even further improvement to the overall design of the connector. For the first study, there was a limitation in that as the corner radius increased, so, too, did the volume of the central junction, thus giving more opportunity for turbulent flow and recirculation areas. Thus, the corner radius range had to be limited. In the second study, the diverter was added to the already optimized corner radius connector to try to eliminate the central recirculation area, which was reasonably successful. However, because the diverter itself reduced the area in the connector through which the blood could flow, it two was limited in its ranges and shapes. Should a secondary study attempt to combine these two studies, the parameter ranges for the corner radius and the diverter could be greatly increased, because the addition of the diverter would solve the central junction volume problem and the larger range of the corner radius would solve the decreasing volume problem for the diverter. This would, in theory, create the most suitable geometry for each of the age groups and could even result in a geometry with corner radii as extreme as that found in the study by Soerensen et al [9].

This could then lead to the creation of a better version of the dual propeller proposed by Jagani et al, based on this new optimized connector. The combination of a superior optimized connector with the option of an active assist device like the dual propeller could effectively replace the need for a heart transplant for patients suffering from right ventricle dysfunction. Thus not only drastically improving the quality of life for patients with right ventricle dysfunction, but also increasing the number of hearts available for transplant for patients suffering from other congenital heart diseases.

6 References

[1] Q. Yang, H. Chen, A. Correa, O. Devine, T. J. Mathews and M. A. Honein, "Racial differences in infant mortality attributable to birth defect in the united states, 1989-2002," *Birgh Defects Research Part A: Clinical and Molecular Teratology,* vol. 76, no. 10, pp. 706-713, 2006.

[2] S. M. Gilboa, J. L. Salemi, W. N. Nembhard, D. E. Fixler and A. Correa, "Mortality Resulting from Dongenital Heart Disease Amond Children and Adults in the United States 1999 to 2006," *Circulation,* vol. 122, pp. 2254-2263, 2010.

[3] "Single Ventricle Defects," Boston Children's Hospital, 2005. [Online]. Available: http://www.childrenshospital.org/conditions-and-treatments/conditions/s/single-ventricle-defects/overview. [Accessed 15 March 2018].

[4] Y. d'Udekem, A. J. Iyengar, A. D. Cochrane, L. E. Grigg, J. M. Ramsay, G. R. Wheaton, D. J. Penny and C. P. Brizard, "The Fontan Procedure: Contemporary Techniques Have Improved Long-Term Outcomes," *Circulation,* pp. I-157-I-164, 2007.

[5] E. Be'eri, S. E. Maier, M. J. Landzberg, T. Chung and T. Geva, "In Vivo Evaluation of Fontan Pathway Flow Dynamics by Multidimensional Phase-Velocity Magnetic Resonance Imaging," *Circulation,* vol. 98, pp. 2873-2882, 1998.

[6] F. Fontan and E. Baudet, "Surgical repair of tricuspid atresia," *Thorax,* vol. 26, no. 3, pp. 240-248, 1971.

[7] M. S. Lemler, W. A. Scott, S. R. Leonard, D. Stromberg and C. Ramaciotti, "Fenestration Improves Clinical Outcome fo the Fontan Procedure," *Circulation,* vol. 105, pp. 207-212, 2002.

[8] J. Jagani and A. Untaroiu, "A Study of TCPC-Stent Conjunction for Cavopulmonary Assist in Fontan Patients with Right Venticular Dysfunction," in *International Mechanical Engineering Congress and Exposition*, Phoenix, Arizona, 2016b.

[9] D. D. Soerensen, K. Pekkan, D. de Zélicourt, S. Sharma, K. Kanter, M. Fogel and A. P. Yoganathan, "Introduction of a New Optimized Total Cavopulmonary Connection," *The Annals of Thoracic Surgery,* vol. 83, no. 6, pp. 2182-2190, 2007.

[10] A. L. Marsden, A. J. Bernstein, M. V. Reddy, S. C. Shadden, R. L. Spilker, F. P. Chan, C. A. Taylor and J. A. Feinstein, "Evaluation of a novel Y-shaped extracardiac Fontan baffle using computational fluid dynamics," *The Journal of Thoracic and Cardiovascular Surgery,* vol. 137, no. 2, pp. 394-403, 2009.

[11] J. Jagani, "Dual Propeller Micro-Pump and TCPC Smart Connector for superior Hemodynamics and Cavopulmonary Support". United States of America Patent 62/422,117, 11 15 2016a.

[12] J. N. Jagani, "Design of Percutaneous Dual Propeller Pump to assist Patients with single Functional Ventricle," Jakin Nitin Jagani, Blacksburg, Virginia, 2018.

[13] B. K. Bharadvaj, R. F. Mabon and D. P. Giddens, "Steady Flow ina Model of the Human Carotid Bifurcation. Part 1 - Flow Visualization," *Journal of Biomechanics,* vol. 15, no. 5, pp. 349-362, 1982.

[14] E. W. Merrill and G. A. Pelletier, "Viscosity of human blood: transition from Fewtonian to non-Newtonian," *J. appl. Phystol.,* vol. 23, pp. 178-182, 1967.

[15] A. Untaroiu, H. Wood and P. Allaire, "Artificial Heart Pump Flow Path Design: Cfd Modeling and Experimental Validation of Flow Performance," *Artificial Organs,* vol. 33, no. 6, p. A89, 2009a.

[16] A. Untaroiu, H. G. Wood and P. E. Allaire, "Numerical evaluation of blood damage in a magnetically levitated heart pump - biomed 2009," *Biomedical sciences instrumentation ,* vol. 45, pp. 220-225, 2009b.

[17] S. Kutty, L. Li, R. Hasan, Q. Peng, S. Rangamani and D. A. Danford, "Systemic Venous Diameters, Collapsibility Indices, and Right Atrial Measurments in Normal Pediatric Subjects," *Journal of the American Society of Echocardiography,* vol. 27, no. 2, pp. 155-162, 2014.

[18] Z. Knobel, C. J. Kellenberger, T. Kaiser, M. Albisetti, E. Bergstrasser and E. R. Valsangiacomo Buechel, "Geometry and dimensions of the pulmonary artery bifurcation in children and adolescents: assessment in vivo by contrast-enhanced MR-angiography," *International Journal of Cardiovascular Imaging,* vol. 27, pp. 385-396, 2011.

[19] M. A. Salim, T. G. DiSessa, K. L. Arheart and B. S. Alpert, "Contribution of Superior Vena Caval Flow to Total Cardiac Output in Children".

[20] C. P. Cheng, R. J. Herfkens, A. L. Lightner, C. A. Taylor and J. A. Feinstein, "Blood flow conditions in the proximal pulmonary arteries and vena cavae: healthy children during upright cycling exercise," *American Journal of Physiology Heart Circulation Physiology,* vol. 287, pp. H921-H926, 2004.

[21] S. Ovroutski, S. Nordmeyer, O. Miera, P. Ewert, K. Klimes, T. Kuhne and F. Berger, "Caval Flow Reflects Fontan hemodynamics: quantification by magnetic resonance imaging," *Clin. Res. Cardiol,* vol. 101, pp. 133-138, 2012.

[22] C. P. Cheng, R. J. Herfkens, C. A. Taylor and J. A. Feinstein, "Prozimal Pulmonary Artery Blood Flow Characteristics in Healthy Subjects Measured in an Upright Posture Using MRI: The Effects of Exercise and Age," *Journal of Magnetic Resonance Imaging,* vol. 21, pp. 752-758, 2005.

[23] C. P. Appleton, L. K. Hatle and R. L. Popp, "Superior Vena Cava and Hepatic Vein Doppler Enchocardiography in Healthy Adults," *JACC,* vol. 10, no. 5, pp. 1032-1039, 1987.

[24] L. Wexler, D. H. Bergel, I. T. Gabe, G. S. Makin and C. J. Mills, "Velocity of Blood Flow in Normal Human Venae Cavae," *Circulation Research,* vol. 23, pp. 349-359, 1968.

[25] G. Kovacs, A. Berghold, S. Scheidl and H. Olschewski, "Pulmonary arterial pressure during rest and exercise in healthy subjects: a systematic review," *European Respiratory Journal,* vol. 34, pp. 888-894, 2009.

[26] R. D. Rowe and L. S. James, "The Normal Pulmonary Arterial Pressure During The First Year of Life," *The Journal of Pediatrics,* vol. 51, no. 1, pp. 1-4, 1957.

[27] N. O. Fowler, R. N. Westcott and R. C. Scott, "Normal Pressure in the Right Heart and Pulmonary Artery," *American Heart Journal,* vol. 46, no. 2, pp. 264-267, 1953.

[28] E. G. Lakatta, J. H. Mitchell, A. Pomerance and G. G. Rowe, "Characteristics of Specific Cardiovascular Disorders in the Elderly, Human Aging: Changes in Structure and Function," *JACC,* vol. 10, no. 2, pp. 42A-47A, 1987.

[29] E. Mack and A. Untaroiu, "Hemodynamics Characteristics of a Four-Way Right-Atrium Bypass Connector," in *Fluids Engineering Division Summer Meeting*, Waikoloa, Hawaii, 2017.

[30] A. Untaroiu, H. G. Wood and P. E. Allaire, "Implantable axialflow blood pump for left ventricular support," *Biomedical Sciences Instrumentation,* vol. 44, pp. 310-315, 2007.

[31] H. G. Wood, A. L. Throckmorton, A. Untaroiu and X. Song, "The medical physics of ventricular assist devices," *Reports on Progress in Physics,* vol. 68, no. 3, p. 545, 2005.

[32] S. M. Patel, A. L. Throckmorton, A. Untaroiu, P. E. Allaire, H. G. Wood and D. B. Olsen, "The status of Failure and reliability testing of artificial blood pumps," *2005,* vol. 51, no. 4, pp. 440-451, ASAIO Journal.

[33] A. L. Throckmorton and A. Untaroiu, "CFD analysis of a Mag-Lev ventricular assist device for infants and children: Fourth generation design," *ASAIO Journal,* vol. 54, no. 4, pp. 423-431, 2008.

[34] "Genetic Aggregation," SAS IP, Inc., [Online]. Available: https://www.sharcnet.ca/Software/Ansys/17.0/en-us/help/wb_dx/dxTheoGeneticAgg.html. [Accessed 22 February 2017].

[35] N. Marco, J. A. Desideri and S. Lanteri, "Multi-Objectiver Optimization in CFD by Genetic Algorithms," 1999.

[36] "Multi-Objective Genetic Algorithm (MOGA)," SAS IP, Inc., [Online]. Available: https://www.sharcnet.ca/Software/Ansys/17.0/en-us/help/wb_dx/dxBEMtemp11.html#dx_theory_MOGAPopulation. [Accessed 22 February 2017].

[37] K. H. Fraserr, T. Zhang, M. E. Taskin, B. P. Griffith and Z. J. Wu, "A Quantitative Comparison of the Mechanical Blodd Damage Parameters in Rotary Ventricular Assist Devices: Shear Stress, Exposure Time and Hemolysis Index," *Journal of Biomechanical Engineering,* vol. 134, no. 8, pp. 0810021-08100211, 2012.

[38] A. Untaroiu, H. G. Wood and P. E. Allaire, "Implantable axialflow blood pump for left ventricular support," *Biomedical Sciences Instrumentation,* vol. 44, pp. 310-315, 2007.

[39] H. G. Wood, A. L. Throckmorton, A. Untaroiu and X. Song, "The medical physics of ventricular assist devices," *Reports on Progresss in Physics,* vol. 68, no. 3, p. 545, 2005.

[40] S. M. Patel, A. L. Throckmorton, A. Untaroiu, P. E. Allaire, H. G. Wood and D. B. Olsen, "The status of failure and reliability testing of arificial blood pumps," *ASAIO Journal,* vol. 51, no. 4, pp. 440-451, 2005.

[41] M. Giersiepen, L. J. Wurzinger, R. Opitz and H. Reul, "Estimation of shear stress-related blood damage in heart valve prostheses--in vitro comparison of 25 aortic valves," *The International journal of artificial organs,* vol. 13, no. 5, pp. 300-306, 1990.

[42] M. E. Taskin, K. H. Fraser, T. Zhang, C. Wu, B. P. Griffith and Z. J. Wu, "Evaluation of Eulerian and Lagrangian models for hemolysis estimation," *ASAIO journal,* vol. 58, no. 4, pp. 363-372, 2012.

[43] K. H. Fraser, T. Zhang, M. E. Taskin, B. P. Griffith and Z. J. Wu, "A quantitative comparison of mechanical blood damage parameters in rotary ventricular assist devices: shear stress, exposure time and hemolysis index," *Journal of biomechanical engineering,* vol. 134, no. 8, p. 081002, 2012.

[44] A. H. Association, "Executive Summary: Heart Disease and Stroke Statistics-2015 Update," American Heart Association. Inc., Dallas, TX 75231, 2016.

[45] D. T. Hsu and G. D. Pearson, "Heart Failure in Children Part 1: History, Etiology, and Pathophysiology," American Heart Association, Dallas, TX, 2009.

[46] A. L. Throcknorton, S. Lopez-Isaza, E. A. Downs, S. G. Chopski, J. J. Gangemi and W. Moskowitz, "A Viable Therapeutic Option: Mechanical Cirgulatory Support of the Failing Fontan Physiology," *Pediatric Cardiology,* pp. 1357-1365, 2013.